

Review

# Heat Transfer Considerations on the Spontaneous Triggering of Vapor Explosions—A Review

Arne Simons <sup>1,\*</sup>, Inge Bellemans <sup>1</sup>, Tijl Crivits <sup>2</sup> and Kim Verbeken <sup>1,\*</sup>

<sup>1</sup> Department of Materials, Textiles and Chemical Engineering, Ghent University, Technologiepark 46, 9052 Ghent, Belgium; Inge.Bellemans@UGent.be

<sup>2</sup> Umicore R&D, 2250 Olen, Belgium; Tijl.Crivits@eu.umicore.com

\* Correspondence: arne.simons@ugent.be (A.S.); kim.verbeken@ugent.be (K.V.)

**Abstract:** Vapor explosions have been investigated both theoretically and experimentally for several decades, focusing either on the vapor film, or on mechanical aspects. Where the main interest for industry lies in the safety risks of such an event, fundamental research is focusing on all partial processes that occur during a vapor explosion. In this paper, vapor explosions are discussed from a heat transfer point of view. Generally accepted knowledge of heat transfer between hot surfaces and liquids is compared to early investigations regarding the origin of vapor explosions. Both steady state and transient models are discussed. The review of available literature suggests that vapor explosions trigger spontaneously by the collapse of the boiling film. Better understanding of the fundamental aspects of vapor explosions might give rise to future ideas on how to avoid them.

**Keywords:** vapor explosions; melt-coolant interactions; heat transfer; material properties



**Citation:** Simons, A.; Bellemans, I.; Crivits, T.; Verbeken, K. Heat Transfer Considerations on the Spontaneous Triggering of Vapor Explosions—A Review. *Metals* **2021**, *11*, 55. <https://doi.org/10.3390/met11010055>

Received: 10 July 2020

Accepted: 23 December 2020

Published: 29 December 2020

**Publisher's Note:** MDPI stays neutral with regard to jurisdictional claims in published maps and institutional affiliations.



**Copyright:** © 2020 by the authors. Licensee MDPI, Basel, Switzerland. This article is an open access article distributed under the terms and conditions of the Creative Commons Attribution (CC BY) license (<https://creativecommons.org/licenses/by/4.0/>).

## 1. Introduction

Many applications used in industry and in daily life need cooling to work properly. Water is often used in industrial context as a coolant, thanks to its abundance and excellent cooling properties, such as a high heat capacity ( $C_{p,H_2O} = 4183 \text{ J/kgK}$  [1]) and a high enthalpy of evaporation ( $\Delta H_{evap} = 2.260 \times 10^6 \text{ J/kg}$  [1]). The latter is useful whenever the cooled system has a temperature above the boiling point, since it allows cooling without loss of efficiency.

However, steam explosions are known to occur when bringing hot liquid materials in contact with volatile liquids. This phenomenon occurs in different industries, including the nuclear industry, where it is often referred to as a “fuel-coolant interaction” (FCI) [2,3], the metallurgical industry [4,5], the paper industry [6,7], and the transportation of cryogenic liquids where water acts as the hot liquid [7]. Within the metallurgical industry, a direct contact between the coolant and the pyrometallurgical melt can occur during granulation, charging of the furnace with wet resources or whenever there is a leakage of coolant into the furnace. In the first case, the melt is added to a larger mass of coolant, whereas, in the latter two cases, the coolant is added to a larger mass of melt.

To the best of the authors' knowledge, one of the last review papers on this subject was written by Berthoud [8] in 2000 and focused on the mechanical behavior of vapor explosions. Few review papers have been published since, such as Reference [9–12], but these discuss the available experimental technical bases, the modeling of vapor explosions on large scale or experiments specifically for the nuclear sector, while we intend to tackle the influence of heat transfer on the spontaneous triggering of vapor explosions on a smaller scale, specifically.

Another earlier review paper was written by Fletcher, who mentioned, already at that time, that the number of studies regarding the fundamental bases of vapor explosion triggering had decreased [13]. Even though a lot can still be learned from fundamental research on this topic, today, studies are mainly focusing on the practical side of this

phenomenon, namely on the behavior rather than on the origin of vapor explosions. Examples of these studies include Reference [14,15], two references that provide a means to prevent vapor explosions. However, even though the work within these studies is high-level, these are empirical and qualitative studies rather than fundamental and quantitative ones. That is why the scope of the current paper is to give an overview of the more fundamental theories on the origin of vapor explosions from a heat transfer perspective, in an attempt to revitalize this more fundamental research, possibly leading to a better understanding on the prevention of vapor explosions.

Research of vapor explosions has been executed in several configurations: hot [16] and cold [17] droplet impingement, hot [3] and cold [18] jets, and stratified layers [19]. A certain material under a range of conditions might cause an explosion in one of these configurations but not in another, proving the relevance of the configuration used. This work is written from the perspective of ‘hot droplet impingement’ (i.e., a hot droplet impinging with a large amount of coolant), and the described models and ideas are only relevant to this configuration, unless stated otherwise. After the interactions, the debris usually has sizes ranging from 10  $\mu\text{m}$  to several 100  $\mu\text{m}$  [15,20]. Furthermore, the heat transfer involved in these interactions has been studied mathematically, often using steady-state models. These models include a liquid or solid sphere, which is placed in a moving liquid coolant. This represents a dispersed phase flow in which discrete droplets/particles of one phase are present in a continuous mass of the other phase [21]. Typical dimensions of these droplets/particles are in the order of magnitude of millimeters [16,20], which can be implemented in dimensionless numbers generally used to describe systems of multiphase flow.

Today, there is a general agreement that a vapor explosion in practice occurs in multiple steps: premixing, triggering, propagation and expansion [22–25]. A schematic overview of these steps can be seen in Figure 1. During small scale experiments with a single droplet of the hot phase, there is practically no premixing (step (1) in Figure 1) since the geometry already consists of a small droplet. As such, the interaction starts with deformation of the droplet, triggering an explosion (step (2) in Figure 1). An explosion can be triggered both by thermodynamic and hydrodynamic effects. We argue this is an incorrect use of the word ‘thermodynamic’, and we will be referring to this triggering as ‘thermal triggering’ in the rest of this paper.

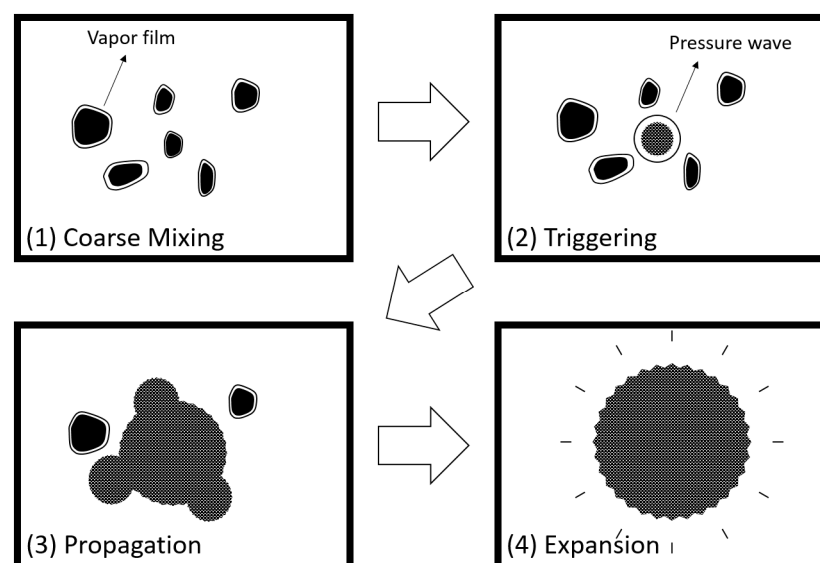


**Figure 1.** Schematic overview of the steps by which a vapor explosion occurs (adapted from Reference [22]).

Hydrodynamic fragmentation models are inappropriate in small-scale configurations, such as 1-droplet experiments, since there appears to be not enough slip flow [16]. That is why the focus of this paper will be on thermal fragmentation models. Once the trigger has occurred, a cyclic process is started in larger systems (the propagation, step (3) in Figure 1), in which a local explosion creates a pressure wave which functions as a trigger for a subsequent explosion. At some point, the contact area is so large that a final explosion will occur (step (4) in Figure 1).

In the remainder of this paper, the origin of step 2, the ‘trigger’ of the explosion, will be considered from a heat transfer point of view. First, initial studies about vapor explosions will be discussed. Next, the results of these studies are explained using knowledge on heat transfer from before that time. These explanations are then critically discussed, resulting in suggestions for future research.

## 2. History of Studies Regarding Vapor Explosions

Vapor explosions have been investigated both conceptually and experimentally since 1970 [26] (older observations exist, but it had not been named as such nor was there any explicit research regarding the phenomenon itself). In conceptual investigations, theoretical principles and model equations are used to study the following questions: how and why does this interaction occur? Experimental studies, on the other hand, are more practical and were performed to investigate which parameters have an influence on the phenomenon. These studies intended to learn how to control the behavior, rather than to understand why it is happening. The following sections first discuss the conceptual research, followed by more recent studies investigating the influencing parameters.

### 2.1. Nature of a Vapor Explosion

Explosions (including steam explosions) had always been linked with chemical reactions. However, in the fifties, it was found that non-reactive metals also show vapor explosions [26,27] and that reactive metals only react for a fraction of the used mass [26,28]. Furthermore, Long [29] did not observe any flash, which is characteristic for the fast detonation in a chemical explosion, in his experiments with large quantities of molten aluminum in water, where a chemical reaction was generally expected. Later reports about vapor explosions with aluminum where a spontaneous interaction occurred can be found [30–33]. These reports noticed an increase in heat transfer through the vapor film, which could possibly be caused by the production of H<sub>2</sub> by chemical reactions. However, this hypothesis could not be proved [31]. Furthermore, flashes of white light have been observed for experiments with aluminum [33], but other researchers also mention that chemical reactions seemed unlikely as the explosive interaction for experiments with aluminum and copper were very similar [34,35]. Due to these observations, the idea of a physical reaction gained more followers. However, a theoretical study by Epstein [36] combined with experimental results of Higgins [37] revealed that each collision between water molecules and metal atoms would have to interact physically to justify the rapid nature of the phenomenon. In 1970, Witte et al. [26] published a paper discussing the explosive triggering of vapor explosions. The only explanation for these fast reactions is that fragmentation would cause an increase in contact area. Fragmentation needs a trigger to be able to overcome the surface energy corresponding to the increase in surface area. Initially, there were 4 theories for the triggering of fragmentation of a droplet of pyrometallurgical phase falling into a large pool of coolant [26]:

1. Entrapment: a rapid evaporation of coolant being trapped between the hot phase and the container which blows apart the hot phase [29].
2. Violent boiling: forces originating from the rapid production and release of vapor bubbles (transition from film boiling to nucleate boiling) tear apart the hot phase [38].
3. Shell theory: a rapid evaporation of coolant suddenly being trapped inside the hot phase which blows apart the hot phase [39].

4. Weber number effect: the forces originating from the relative movement between the coolant and the hot phase tear apart the hot phase [40,41].

It is pointed out that more than one of these hypotheses might be correct, or that there might be a synergetic combination of triggers. The first three of the above hypotheses include the boiling regime in one way or another, which will be discussed in Section 3. Based on the observations in a later study by Witte et al. [42], some modifications of the existing hypotheses on fragmentation were required. For example, during transition boiling the vapor film collapses and reforms with an oscillation time of a few milliseconds, as was observed in earlier experimental work on transition boiling around solid, spherical particles by Stevens et al. [43]. However, Witte et al. [42] found that complete fragmentation occurred in a slightly longer timeframe. As such, if transition boiling has any effect on fragmentation, it is via the initial vapor film collapse. Violent boiling during transition boiling appears to be insignificant (i.e., change above-mentioned hypothesis 2 from ‘Violent boiling’ to ‘Initial film collapse’).

Furthermore, the shell theory also seems rather unlikely. High-speed photography showed a vapor film surrounding the hot droplet just one frame prior to the onset of fragmentation, and it is very unlikely that the coolant penetrated both the vapor film and the droplet in such a short time span. Lastly, the Weber number effect does not appear to have a major influence since fragmentation only occurred once the hot phase reached a certain depth, rather than shortly after penetrating the water. With these results, Witte et al. [42] disproved three of the main hypotheses of that moment. As such, almost all initial hypotheses required adaptations to remain viable.

‘Entrapment’ was the only unchanged hypothesis remaining from the original set, but it is currently known that it can be inhibited by the application of highly non-wetting coatings [44]. Furthermore, it was found from experiments that ‘entrapment’ cannot be the only viable mechanism as explosions have been observed in bulk coolant [15,16,45]. Hence, there was interest in the development of adapted or new hypotheses. For instance, Witte et al. [46] suggested a new hypothesis, namely ‘the shrinking shell theory’. This hypothesis considers a pressure buildup inside the hot droplet due to solidification and shrinkage of the exterior of the droplet, resulting in a bursting of the solidified crust.

Other conclusions by Witte et al. [26] include that the droplet was certainly in the molten state at the onset of fragmentation, and that the trigger should possibly be external. The latter was concluded because when multiple droplets fell into a tank of water, fragmentation of one such droplet seemed to trigger the sequential fragmentation of other neighboring droplets. If triggering of every single droplet was internal, then the fragmentation of different droplets would be uncorrelated. Only the initial trigger could still be internal. All above observations lead to newly proposed hypotheses on how to trigger fragmentation, most of them being related to causing an imbalance. It is assumed that the droplet is kept together by the surface tension, as shown in the following equation:

$$P_{in} - P_{ex} = \frac{4\sigma}{D}, \quad (1)$$

where  $P_{in}$  and  $P_{ex}$  represent the interior and exterior pressure, respectively,  $D$  is the diameter of the droplet, and  $\sigma$  is the surface tension between the droplet and its surroundings. From this equation, it can be seen that an imbalance can originate from a change in pressure inside or outside the droplet, from a change in surface tension, or a change in droplet size. The latter is unlikely to occur before any of the others has occurred, resulting in the following proposed mechanisms for fragmentation:

1. Fragmentation by entrapment near boundaries: this hypothesis remains the same as before, coolant is being trapped between the hot phase and the container. As such, it evaporates and blasts apart the hot droplet.
2. Fragmentation by vapor film collapse: these are the newly formed hypotheses originating from the transition of film boiling to nucleate boiling. This transition causes the vapor layer to disappear, resulting in some possible mechanisms for fragmentation:

- a. Pressure imbalance (outward): the vapor film condensates at its outer boundary. The created void is being filled both by the surrounding liquid coolant and the vapor. Since the vapor has a lower density, it moves faster, expanding its volume. As such, the pressure around the hot droplet decreases and the droplet expands and fragments.
- b. Pressure imbalance (impact): the vapor film condensates at its outer boundary and creates a cavity. The surrounding coolant is being sucked into the cavity and will eventually impact the hot droplet symmetrically. This impact causes a compressive pressure pulse in the droplet, which reflects in the center and becomes a diverging wave moving radially outward. This wave also causes an imbalance in pressure.
- c. A decrease in surface tension  $\sigma$ :  $\sigma$  is determined by the present phases. If the vapor phase is replaced by a liquid coolant phase, this corresponds to a change in  $\sigma$ . This changes the forces keeping the droplet together and might result in fragmentation.
- d. Thermal shock: heat transfer through the vapor layer occurs mainly by convection and conduction. Once the vapor layer has a sufficiently small thickness, the heat flux leaving the hot droplet becomes that high that the outer part of the droplet can cool down rapidly and experience a thermal shock, resulting in fragmentation.

All above-mentioned mechanisms are induced by a continuous decrease in temperature, but there might be other causes related to geometric effects or even effects which are still unknown.

## 2.2. Influence of Surroundings on Explosion Behavior

Zyszkowski [47] studied the cooling behavior of molten copper in water as a function of the atmospheric parameters (normal air vs. inert gas), in an attempt to study the Leidenfrost temperature. Initially, he observed two different kinds of behavior: 'thermal explosion' and 'normal course'. The latter ends with a 'transplosion', a seemingly explosive ending of the film boiling regime (also see Sections 2.3 and 3.3). In a subsequent study [48], he also observed a different kind of behavior, namely 'Empty shell particles' (see Figure 2). In all cases, the first observed event, as shown in Figure 2, is the moment when the droplet reaches the bottom of the tank. The thermocouple in the bottom registers this contact, and the temperature reaches its maximum value (point A in Figure 2). From here on, the three different courses separated, all having a different transition point  $L/L'/L''$  (i.e., the Leidenfrost temperature). In the specific case of thermal explosion, a jet (in order not to mistake this for the jet configuration, it will be called a protrusion in the continuation of this paper) is observed prior to explosion. The protrusion forms approximately at point B, triggers a direct contact between the melt and the liquid coolant and results in a sudden drop in temperature. Fragmentation follows, and the actual explosion then occurs somewhere between point B and C. Once the explosion has passed, the debris solidifies, and, apparently, a new vapor film is formed, which then destabilizes at point  $L'$ . Finally, it should be noted that, whenever the sample was molten/heated under an inert gas, only the 'Normal course' occurred.

In addition, more recent studies investigated the influence of the environment on the material. An example of such a study was performed by Zielinski et al. [15]. In their study with droplet impingement, they observed that aluminum and gallium did not show spontaneous explosions, whereas tin and galinstan did. Furthermore, the addition of trace amounts of aluminum (0.3 wt%) to galinstan inhibits spontaneous interactions. Zielinski et al. [15] mentioned that this is probably due to the production of non-condensable gasses during the oxidation of the aluminum. The accompanying  $H_2$  evolution results in the prevention of the triggering onset. In addition, other researchers also mentioned the inhibition of vapor explosions by non-condensable gasses [49]. On the other hand, the addition of 10 wt% of NaCl to the water made experiments with galinstan even more

energetic, and it also caused a possible spontaneous interaction in experiments with gallium. Other research on the influence of salt additions was performed by Furuya and Kinoshita [22]. In their experiments with the impingement of a droplet of coolant on top of a bath of hot phase (rather than melt into coolant), they observed that for a constant coolant temperature, the temperature range for spontaneous interactions moves to higher initial temperatures of the hot phase with the addition of salts. Later, Furuya and Arai [14] also showed that the quenching temperature (i.e., the temperature of the hot phase at which the vapor film collapses) was increased with the addition of salt. The influence of the initial temperature on this quenching temperature was not investigated; thus, a link with the temperature range for spontaneous interaction could not immediately be provided. More on this temperature range will be discussed in the next section.

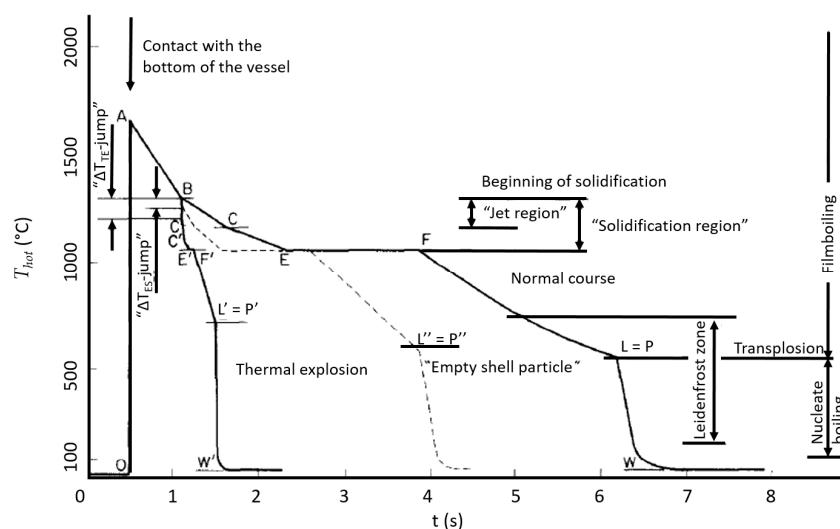


**Figure 2.** Possible cooling curves (temperature of the hot phase ( $T_{hot}$ ) measured at the bottom (Y-axis) versus time (X-axis)) for 1 g of molten copper in water (adapted from Reference [48]).

### 2.3. Influence of Temperature on Explosion Behavior

Another investigation [50] studied horizontal jets of molten metal in a water tank. Conditions were optimized to inhibit hydrodynamic effects, as to investigate solely thermal fragmentation. The main observation was the influence of the injection temperature ( $T_{inj}$ ). At low  $T_{inj}$ , the melt would solidify before any interaction could occur. When  $T_{inj}$  was increased, while keeping the same composition, the melt solidified, while the gas was expanding to a certain extent (see Figure 3A), causing porous, popcorn-like debris. At even higher temperatures, the melt fragmented completely.  $T_{inj}$  also influenced the ‘distance to explosion’, comparable to the depth of the explosion in impingement experiments, as can be seen in Figure 3B. The decreasing distance to explosion with increasing  $T_{inj}$  might seem illogical if one assumes that triggering will occur as soon as the temperature of the melt drops below a certain critical value. However, this phenomenon was not further discussed by Bradley and Witte [50].

Bradley and Witte [50] also studied the timeline of the interaction and found that jet expansion took roughly 750  $\mu$ s, followed by breakdown (in case of an explosion) which took 200  $\mu$ s to 500  $\mu$ s. Finally, they investigated the heat flux during the interaction. They calculated the heat flux from the time to solidify, the average ratio of volume over surface of the melt, the latent heat and the initial temperature (i.e., energy) of the melt. They found an increase in heat flux with increasing initial temperature ( $T_{ini}$ ). However, the heat flux increased faster than would be expected for flow around a solid. They mention that the heat flux was inversely proportional to the expansion of the jet, which can be understood as the latter caused an increase in surface area (an effect which is not encountered with a solid sphere).

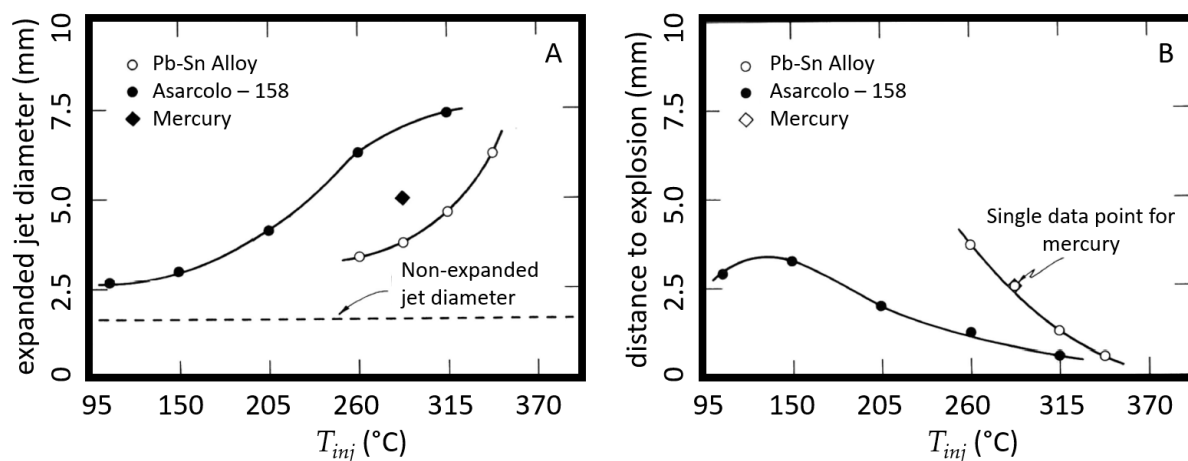


**Figure 3.** Experimental data of the influence of the injection temperature ( $T_{inj}$ ) for different materials on (adapted from Reference [50]): (A) Jet expansion; (B) distance to explosion.

It was impossible for Bradley and Witte [50] to prove any existing or develop a new mechanism for the fragmentation, but they were able to draw some conceptual conclusions:

1. Explosions were observed when the melt was in the liquid state and even when no solidification took place, e.g., superheated mercury will still fragment without reaching its solidification temperature [50], which was also recently observed by the authors of this work [51]. Hence, solidification is not required for fragmentation of the droplet, making ‘the shrinking shell theory’ only a secondary possibility [52].
2. Secondly, Bradley and Witte [50] mention that rapid evaporation of coolant trapped inside the droplet seems very unlikely as there is no sign of coolant penetrating the jet.
3. Furthermore, it is mentioned that the violence of transition-nucleate boiling could not be a necessity for fragmentation since fragmentation also occurs at temperatures of the hot phase ( $T_{hot}$ ) below the boiling point of water (the reader is again referred to experiments with mercury). Our opinion is that the fragmentation of mercury might occur because of hydrodynamic effects since the latter happen at any temperature.
4. Bradley and Witte [50] could also conclude from their observations that the oscillation time during transition boiling is too long as compared to the duration of the explosion. However, they mention that the first film collapse in transition boiling is a possible cause since it takes only a fraction of the time for complete transition. The observation of explosions taking place after film collapse points to this hypothesis.

Lastly, Bradley and Witte [50] performed a dimensional analysis which resulted in the idea that vapor explosions are driven by the cooling rate. Since the heat flux was never measured in this study, they tried to perform a qualitative experiment. They changed the nozzle material from stainless steel to brass, a material with higher thermal conductivity, which will cause the outer layers of the droplet to cool down faster. They saw that tin at a  $T_{hot}$  that caused explosions with a stainless steel nozzle did not show any explosion with the brass nozzle. Rather, it entered the water as a liquid with a colder surface temperature (decreasing the heat flux) and solidified as popcorn-like strands. The change in behavior with decreasing surface temperature could be explained by the decreasing heat flux, since the temperature difference between the surface of the melt and the coolant was decreased. However, we want to note that in the limiting case, the outer shell of the jet solidified, inhibiting all interaction.

Later, Dullforce et al. [53] investigated the influence of the temperature of both the melt ( $T_{hot}$ ) and the coolant ( $T_l$ ) on the explosion behavior. They performed many experiments for different combinations of  $T_{hot}$  and  $T_l$  and they observed that not all of them resulted in an explosion. They found that there is a certain region in which explosions occur, referred to

as the ‘temperature interaction zone’ (TIZ) (see grey area in Figure 4). In their experiments, 12 g of tin was dropped into a tank of water. The droplet cools down, while the coolant keeps a nearly constant temperature. As a result, the combination of  $T_{hot}$  and  $T_l$  moves to the left on an approximately horizontal line. This line might cross the TIZ, so one might expect an explosion anyway (as long as  $T_l$  is sufficiently low). However, that is not how one should read a TIZ. If the cooling curve passes through the TIZ but the initial combination of temperatures lies not within the TIZ, there will be no explosion. This might seem strange but will be discussed later in this review paper. Only if the initial combination of temperatures lies within the borders of the TIZ, an explosion will occur. Witte et al. [26] mention the possible existence of a maximum temperature above which there cannot be any direct contact between the coolant and the hot phase, resulting in a maximum value for the transition temperature. They had the idea that this maximum temperature is equal to the critical temperature of the coolant from the statement of Westwater [54]. However, Westwater only refers to a critical difference in temperature, rather than the critical temperature itself. To the best of our knowledge, no exact value for the maximum contact temperature, i.e., maximum value for the transition temperature, has ever been mentioned in literature.

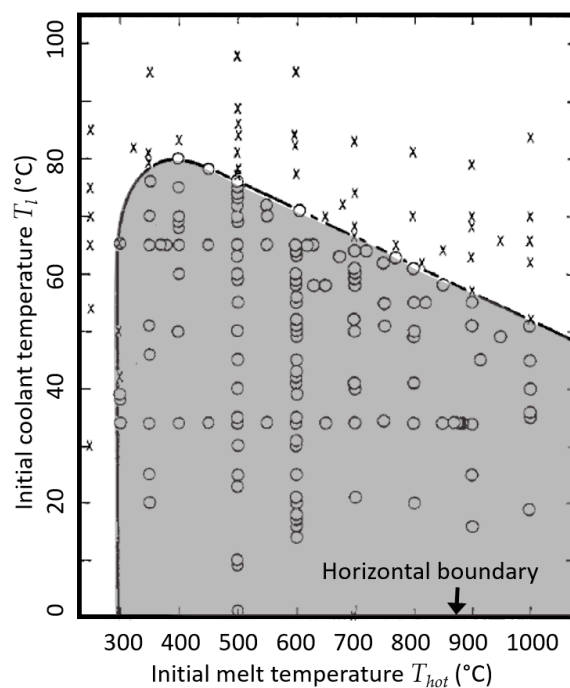


**Figure 4.** Representation of the temperature interaction zone (TIZ, grey area) for the interaction of 12 g of tin with distilled water (adapted from Reference [53]).

From the study of Zyszkowski [47], it was seen that a transpllosion occurs once the contact temperature has dropped below the Leidenfrost temperature. In case of a thermal instability of the film around a hot plate submerged in a liquid pool, the transition temperature is referred to as the minimum film boiling temperature ( $T_{MFB}$ ). On the other hand, in the case of a thermal instability of the film around a separate droplet on top of a plate, the transition temperature is referred to as the Leidenfrost temperature ( $T_{Leid}$ ). Besides this small configurational difference, both have the same meaning: the temperature below which the vapor film becomes unstable. In ideal circumstances,  $T_{Leid}$  is only a function of the properties of the coolant. However, since the hot phase does not have infinitely high heat capacity, density and/or thermal conductivity, the interface temperature will lay between the temperature of the hot and the cold phase. Thus,  $T_{Leid}$  for a hot phase in contact with a certain coolant is a function of the properties of both materials. This function was estimated in both a hydrodynamic and a thermal manner, shown in Equations (3) and

(4), respectively [47]. These equations have also been obtained by other researchers: the hydrodynamic model was also obtained by Berenson [55] for the case of water at its boiling temperature in contact with an isothermal solid, and the thermal model was also obtained by Baumeister and Simon [56]. It should be noted that the hydrodynamic equation was obtained by assuming Rayleigh-Taylor instabilities which only include the acceleration rather than the relative velocity of the phases.

$$\Delta T_{min,ISO} = T_{Leid,ISO} - T_{boil} = 0.127 \frac{\rho_v \Delta H_{evap}}{k_v} \left( \frac{g(\rho_l - \rho_v)}{\rho_l + \rho_v} \right)^{\frac{2}{3}} \left( \frac{\sigma}{g(\rho_l - \rho_v)} \right)^{\frac{1}{2}} \left( \frac{\mu_v}{g(\rho_l - \rho_v)} \right)^{\frac{1}{3}}, \quad (2)$$

$$T_{Leid} = (1 + \theta)(T_{boil} + \Delta T_{min,ISO}) - \theta T_l \text{ where } : \theta = \sqrt{\frac{0.176(k\rho C_p)_l}{(k\rho C_p)_{hot}} \left[ \frac{(\Delta H_{evap} + \frac{C_{p,l}}{2}(T_{boil} - T_l))}{C_{p,hot} \Delta T_{min,ISO}} \right]^{0.6}}, \quad (3)$$

where  $g$  is the local acceleration of gravity,  $\rho_i$  is the density of phase  $i$ ,  $k_v$  is the thermal conductivity coefficient of the vapor,  $\sigma$  is the surface tension between the coolant and its vapor,  $\mu_v$  is the dynamic viscosity of the vapor,  $C_{p,i}$  is the heat capacity of phase  $i$ , and  $T_{Leid,ISO}$  represents the Leidenfrost temperature in ideal circumstances (i.e., with an isothermal hot phase). In Equation (3), an erroneous plus sign was corrected to a minus sign (Equation (2) in Reference [47]). As was explained before, this is not realistic since the hot phase cannot have infinitely high thermal conductivity, heat capacity and/or density. In Equation (3), the variable  $\theta$  implements the temperature drop during direct contact. Note that the actual Leidenfrost temperature would equal the isothermal Leidenfrost temperature when  $\theta$  equals zero, i.e., when the hot phase has infinitely high properties. In Equation (4),  $T_{HN}$  is the homogeneous nucleation temperature, which can be related to the critical temperature ( $T_{crit}$ ), the density of the hot phase  $\rho_{hot}$ , the atomic weight of the hot phase ( $At_{hot}$ ), and the surface tension between the coolant and its vapor  $\sigma$ . Furthermore,  $K$  is determined by the considered contact model, which, for the transient convective cooling, results in a function of  $(k\rho C_p)_{hot}$ . For the origin of these equations, the reader is referred to the work of Zyszkowski [47]. It should be noted that  $K$  is always larger than one; thus, both theoretical correlations (Equations (3) and (4)) predict the Leidenfrost temperature to increase with increasing water temperature  $T_l$ .

$$T_{Leid} = K * T_{HN} + (1 - K) T_l \text{ where } \left\{ \begin{array}{l} K = \frac{1}{\exp\left(\frac{3.056 \cdot 10^6}{(k\rho C_p)_{hot}}\right) \operatorname{erfc}\left(\sqrt{\frac{3.056 \cdot 10^6}{(k\rho C_p)_{hot}}}\right)} \\ T_{HN} = 0.84 T_{crit} \left(1 - \exp\left(\frac{-0.24 \rho_{hot}^{\frac{1}{3}}}{At_{hot}^{\frac{1}{9}} \sigma^{\frac{1}{3}}}\right)\right) \end{array} \right. \quad (4)$$

It can be concluded that a transpllosion will occur at different temperatures for different hot phases. The larger the value of  $(k\rho C_p)_{hot}$ , the closer to the ideal case, the lower the Leidenfrost temperature will be. As such, it seems from the above equations that there should be a (possibly small) influence of the material properties on the Leidenfrost temperature. Material properties might be varied by chemical reaction. As a consequence, Zyszkowski [47] observed that the oxide content of the droplet affected the measured Leidenfrost temperature. A final conclusion by Zyszkowski [47] was that the hydrodynamic correlation appears to be an upper limit for the Leidenfrost temperature. This will be discussed in more detail below.

Kondo et al. [57] further investigated the influence of both the melt temperature and the coolant temperature. They performed experiments in the MELT-II facility and observed different kinds of interaction, depending on the initial conditions. To use the same vocabulary, they will be called interaction modes A, B, C and D, all of which are indicated in Figure 5A. Only interaction modes B and D showed an event with changing pressure (i.e., a vapor explosion) measured by the pressure transducers. Mode A occurs for relatively hot coolant and cold melt phases. It typically has a stable film boiling regime, where the jet can penetrate the water undisturbed (no energetic interaction). Mode B interactions occur when both the coolant and the melt have a relatively high temperature. Multiple pressure pulses

characterize this mode. At even higher melt temperatures, interaction mode C occurs. The vapor production rate is high enough to prevent the film from collapsing; hence, no explosions are observed. At lower coolant temperatures, no vapor film was observed. The interaction in mode D occurs immediately when the jet crosses the water surface, whereas mode B occurred below the water level. The work of Kondo et al. [57] resulted in a new version of Figure 4 (which was obtained for droplet impingement rather than a jet), which can be seen in both images of Figure 5.

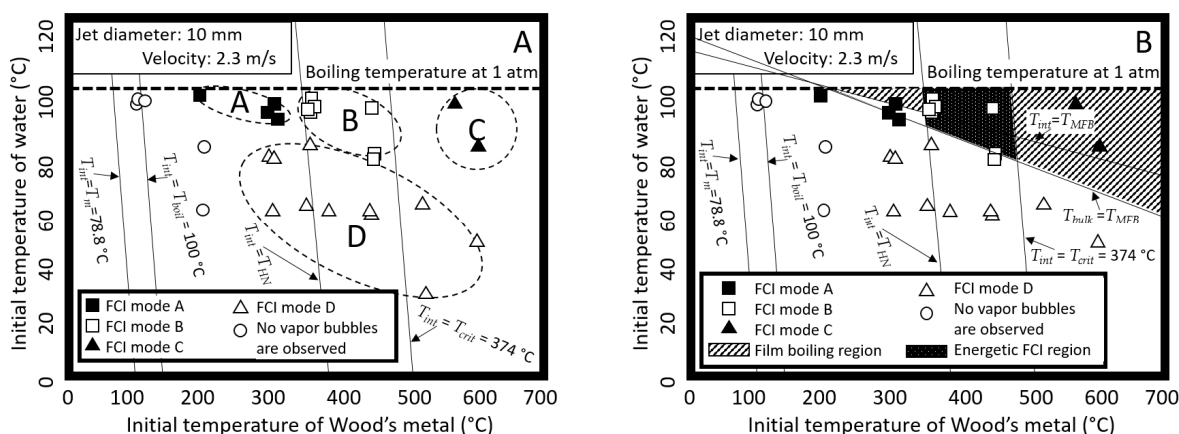


**Figure 5.** Influence of temperature of coolant (Y-axis) and melt (X-axis) on (adapted from Reference [57]): (A) Fuel Coolant Interaction modes assigned to the experimental data points; (B) the same data set with film boiling region indicated (according to minimum film boiling temperature model ( $T_{MFB}$ -model)). In these graphs:  $T_{int}$  is the interface temperature;  $T_m$  and  $T_{bulk}$  are the melting temperature and the bulk temperature of the hot phase;  $T_{boil}$ ,  $T_{HN}$ ,  $T_{crit}$ , and  $T_{MFB}$  are the boiling temperature, the homogeneous nucleation temperature, the critical temperature, and the minimum film boiling temperature of the coolant.

In Figure 5A, the different regions of initial conditions resulting in the different interaction modes are shown. It can clearly be seen that the interaction mode changes when the interface temperature crosses the melting point of the Wood's metal ( $78.8^\circ\text{C}$ ), and it changes again when the interface temperature crosses a certain higher temperature, possibly the critical temperature of the water ( $T_{crit}$ ). However, additional lines are needed to explain the difference between interaction modes B and D and the boundary of interaction modes A and C. These lines were obtained by Kondo et al. [57] by taking another look at the minimum film boiling temperature model ( $T_{MFB}$ -model). Due to the relatively small diameter, they chose to work with the thermal model which was further developed by Baumeister and Simon [56]. In order to derive a new formula within this model, Kondo et al. [57] evaluated two separate cases. If the coolant is at its boiling temperature, a constant (i.e., in steady-state) minimum superheating of the hot phase is needed to sustain film boiling (Equation (5)). Next, in case the coolant has significant subcooling, a necessary condition is that the heat flux leaving the melt should be larger than the heat flux entering the bulk of the coolant (or 'equal to' in case of minimum overheating, as shown in Equation (6)). Combining both equations results in a relation for the minimal superheating of the melt to sustain film boiling (Equation (7)). Depending on the cooling behavior of the melt, the minimum superheating should be considered applicable either to the temperature of the melt bulk or the temperature of the melt interface. Both have been plotted in Figure 5B. The difference between Mode B and D is mainly the position of the interaction, i.e., at the water surface or below the water surface. In Mode D, taking place at the water surface, the vapor film is never stable. This results in many small interactions immediately occurring at the water surface. In Mode B, the vapor film is initially stable. The melt falls into the water and cools down. At a certain time, the vapor film becomes unstable and the entire mass

will react at once. As such, it can be said that Mode B is the most dangerous kind of vapor explosion. Mode D is also a kind of vapor explosion, but it is a less dangerous variety.

$$\Delta T_{min,1} = C \cdot (0.844 T_{crit} - T_{boil}), \quad (5)$$

$$\frac{D}{k_v} \left( k_v \frac{\Delta T_{min,2}}{\delta} + h_r \Delta T_{min,2} \right) = \frac{k_l D}{k_v k_l} (h_{conv} \Delta T_{sub}) \leftrightarrow \left( \frac{D}{\delta_{min}} + Nu_r \right) \Delta T_{min,2} = \frac{k_l}{k_v} Nu_c \Delta T_{sub}, \quad (6)$$

$$\Delta T_{min} = \Delta T_{min,1} + \Delta T_{min,2} = C \cdot (0.844 T_{crit} - T_{boil}) + \frac{\frac{k_l}{k_v} Nu_c \Delta T_{sub}}{\frac{D}{\delta_{min}} + Nu_r} \cong 101 + 4.1 \Delta T_{sub}^{5/4}. \quad (7)$$

Note the difference between Figures 4 and 5: the first one shows experimental lines delineating the area where explosive interactions occur, while the latter shows theoretical lines which seem to define multiple areas. Moreover, the first one shows only interactions below the arc, whereas the latter shows the most intense interactions above the line representing  $T_{MFB}$ . The main difference between both set-ups was that the experiments in Figure 4 were performed with a single droplet of tin, whereas the experiments in Figure 5 used a jet-like introduction of Wood's metal, with continuous addition of material for a certain amount of time. To our opinion the explosions from Figure 4 are all in Mode D, whereas mode B is only possible in experiments with jets. This can be understood since Mode D shows many small explosions as soon as a small amount of the jet has impinged the water, which is similar to only a single droplet impinging the water as compared to a jet. In case of a jet, cooling of the jet occurs in a different way, making more intense interactions possible, even at combinations of  $T_{hot}$  and  $T_l$  that are above the line representing  $T_{MFB}$ . This opinion is supported by three more recent studies. Hansson et al. [16] used droplet impingement and clearly saw that the total impact of a vapor explosion resulting from the impingement of a droplet of hot phase into a bath of coolant increased with decreasing coolant temperature. However, Li et al. [25] used jet impingement and literally mentioned that a vapor explosion was expected by the TIZ theory, but no such event was observed. Rather, they observed multiple small-scale vapor explosions. The coolant temperature in these experiments was always around room temperature. The observation of only small-scale interactions by Li et al. [25], could be expected from the results of Kondo et al. [57], who found that large-scale interactions only occur for higher coolant temperatures. This was also confirmed by another recent study regarding jet impingement by Sibamoto et al. [18]. Even though this work discusses a jet of coolant impinging a bath of melt (rather than melt into coolant), the results also showed that the vapor generation is more vigorous for higher water temperatures. Especially noteworthy is the fact that their test with higher coolant temperature (80 °C) resulted in an interaction that plastically deformed the 1 mm thick stainless steel section walls. This is a clear difference between experiments using droplets or jets. Furthermore, Li et al. [25] investigated the size of the debris. Since they used jets, they considered hydrodynamic models for the fragmentation of the jet. These models depend on the relative velocity between the hot phase and the coolant, which continuously decreases from the moment of impingement until the moment of terminal velocity. They observed that the debris size depended on the initial temperature of the melt. According to the 'critical Weber number theory', this would mean that experiments using a higher  $T_{hot}$  (which had smaller debris) would fragment at a higher relative velocity, which was said to be earlier during the descend of the jet. This means that a higher initial temperature will also interact at a higher temperature, as it has had less time for cooling. They also explicitly mention that the influence of the temperature is not embodied well in current fragmentation models; thus, this clearly needs deeper research.

The effect of material properties on the lines in Figure 5 (Equations (3), (4), and (8)) are represented in Figure 6. The goal of this plot is to present the variability of the equations, in order to see which accuracy is needed during the measurement of the different material properties. The plot assumed material properties for the tin-water system at different

temperatures (annotated by ‘min’ and ‘max’ in Figure 6) that can be found in Table 1. Figure 6A shows the variability of the equation for the interface temperature to be equal to either the homogeneous nucleation temperature  $T_{HN}$  or the critical temperature  $T_{crit}$  of the coolant. In Equation (8),  $T_i$  represents the temperature of phase  $i$  [6,58]. It can be seen that the maximum variation is 30 K.

$$T_{HN(or\ T_{crit})} = \frac{\sqrt{(\rho k C_p)_1 T_1} + \sqrt{(\rho k C_p)_2 T_2}}{\sqrt{(\rho k C_p)_1} + \sqrt{(\rho k C_p)_2}}. \quad (8)$$

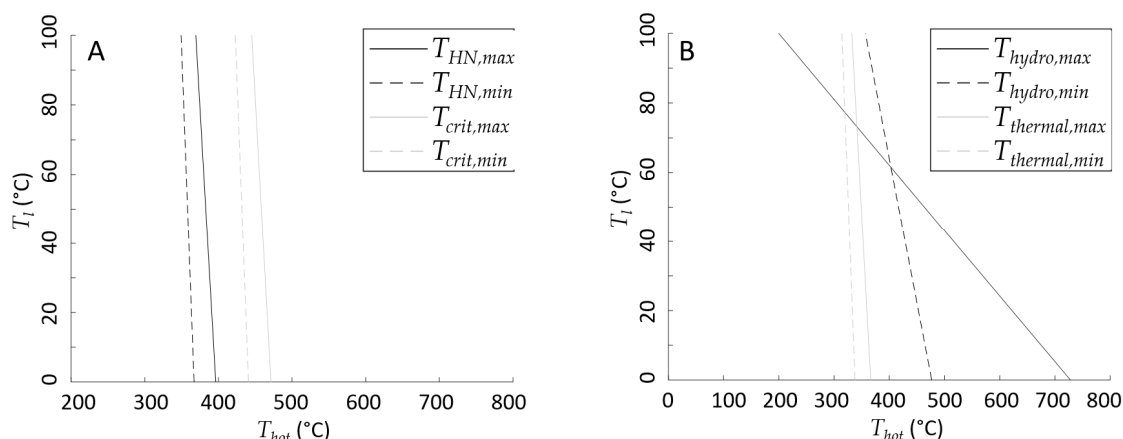


**Figure 6.** Role of material properties in formulas for relevant combinations of melt temperature ( $T_{hot}$ , X-axis) and coolant temperature ( $T_l$ , Y-axis): (A)  $T_{HN}$  and  $T_{crit}$  represent combinations that cause the interface temperature to equal the homogeneous nucleation temperature ( $T_{HN}$ ) and the critical temperature ( $T_{crit}$ ), respectively (Equation (8)); (B) minimum film boiling temperature:  $T_{hydro}$  and  $T_{thermal}$  represent the hydrodynamic (Equation (3)) and thermal model (Equation (4)), respectively. The annotations ‘min’ and ‘max’ relate to higher or lower transition temperature.

**Table 1.** Material properties used to obtain Figure 6.

| Parameter.                         | Min               | Max               | Ref. | Parameter                        | Min      | Max      | Ref. |
|------------------------------------|-------------------|-------------------|------|----------------------------------|----------|----------|------|
| $k_{H_2O}$ [J/(m·s·K)]             | 0.56              | 0.66              | [1]  | $k_{Sn}$ [J/(m·s·K)]             | 25       | 45       | [59] |
| $\rho_{H_2O}$ [kg/m <sup>3</sup> ] | 961.9             | 1000              | [1]  | $\rho_{Sn}$ [kg/m <sup>3</sup> ] | 6300     | 7000     | [60] |
| $C_{p,H_2O}$ [J/(kg·K)]            | 4181              | 4210              | [1]  | $C_{p,Sn}$ [J/(kg·K)]            | 240      | 250      | [61] |
| $k_v$ [J/(m·s·K)]                  | 0.025             | 0.133             | [1]  | $\mu_v$ [Pa·s]                   | 0.000012 | 0.000030 | [1]  |
| $At_{Sn}$ [kg/mol]                 | 0.11871           | 0.11871           | [62] | $\rho_v$ [kg/m <sup>3</sup> ]    | 0.590    | 0.590    | [1]  |
| $\Delta H_{evap}$ [J/kg]           | $2.26 \cdot 10^6$ | $2.26 \cdot 10^6$ | [1]  | $\sigma$ [N/m]                   | 0.0589   | 0.0749   | [1]  |
| $T_{boil}$ [K]                     | 373               | 373               | [1]  | $T_{HN}$ [K]                     | 586      | 586      | [18] |
| $T_{crit}$ [K]                     | 647               | 647               | [1]  |                                  |          |          |      |

Figure 6B represents Equations (3) ( $T_{hydro}$ ) and (4) ( $T_{thermal}$ ). The latter (which was based on thermal principles) again only shows a difference of approximately 30 K. However, the curve of  $T_{hydro}$  (based on the hydrodynamic model) shows a big influence of the properties on the slope of the curve. Since this is the function that was based on hydrodynamic principles, it can be assumed that hydrodynamics will be different for different materials. Furthermore, in droplet impingement experiments, the Leidenfrost temperature is important when the temperature of the melt droplet falls below this temperature. It can clearly be seen in Figure 6B that in most cases, the hydrodynamically derived equation results in a higher value for the Leidenfrost temperature as the black curves are situated on the right side of the plot and will be crossed first when cooling a hot melt droplet in a large amount of coolant at constant temperature. As such, the upper limit for  $T_{MFB}$  is determined by the hydrodynamic model, which was also concluded by Zyszkowski [47]. Only in case the hydrodynamic model is not applicable (e.g., when using small droplets),

the thermal model can be used to find the Leidenfrost temperature. Since vapor explosions can only occur when the hot material is still liquid at the time of vapor film instability, hydrodynamic instabilities are a higher risk. This is because the vapor film will become unstable at higher temperatures, increasing the possibility of it lying above the melting point of the hot phase.

This thermal destabilization of the vapor film is the applicable mechanism in case of temperature gradients starting from room temperature and going up to temperature above the homogeneous nucleation temperature of the coolant. Such temperature profiles occur in investigations regarding Combustion-induced Rapid Phase Transitions (CRPT) [63]. Even though the origin of the explosion in these investigations is different (no need for liquid hot phase), the explosion phenomenon is rather similar to that of vapor explosions. In the experiments performed by Di Benedetto et al. [64,65], water forms through the combustion of methane. This combustion occurs at a flame and results in a high-temperature gas phase. However, the walls of the section are at lower temperature, where water can condensate. Consequently, a temperature gradient exist in the water going from a low temperature at the wall to a high temperature at the free surface. This free surface does not provide any nucleation spots; thus, the water is superheated to its limiting super-heating temperature. Above this temperature, rapid phase transitions occur, similar to the vapor explosions. As such, CRPT is located at the edge between the fields of chemical explosions and physical explosions. More information regarding CRPT can be found in the respective references.

In the above discussions, it was pointed out that there are some observations that could not be explained immediately. The reader is reminded about the influence of the initial temperature of the melt in horizontal jetting experiments, the influence of the surface temperature of the melt in the same experiments, and the influence of the instantaneous temperature in the TIZ and in the decent of jets. Furthermore, the influence of the material properties was obtained theoretically in Equations (3) and (4), but a theoretical approximation that is independent of any material properties was also found (Equation (7)). Some answers to these uncertainties and some deeper knowledge on these phenomena can be found in research towards heat transfer. Furthermore, it had already been noted by Stevens and Witte [66] that vapor explosions probably depend on the destabilization of the vapor film between the hot phase and the coolant [42,50]. A short overview of research regarding heat transfer is given in the next section.

### 3. Overview of Studies on Heat Transfer during Boiling

For the remainder of this review paper, it is important to keep in mind four thermal transport modes [67]:

1. Conduction: Heat diffuses through a stationary material (solid, liquid and/or gaseous).
2. Convection: Heat moves through matter (liquid or gaseous) because of relative motions within.
3. Radiation: Heat is transferred between surfaces or between a surface and a fluid by means of electromagnetic radiation.
4. Phase change: Heat is used for a phase transformation. This is often encountered when a fluid undergoes a liquid-vapor or liquid-solid state transformation near a hot/cold surface. This kind of heat transfer is occurring during boiling and will be further elaborated.

Boiling has been studied for many decades to investigate the surface temperature and heat flux. It is well known that when a volatile coolant is used, the heat flux increases sharply when boiling is initiated [67–70]. This can be seen in the boiling curve, which was first discovered by Nukiyama [71]. Via such a curve, it can be observed that boiling occurs in different regimes, depending on the temperature of the hot zone (see Figure 7). The sudden increase in heat flux when boiling is initiated (point B in Figure 7) can be explained by the promoted convection. The density difference between water and vapor is much larger than the density difference between hot and cold water, hence the rise of bubbles during boiling significantly increases convection. At a certain moment (point D in

Figure 7), the plate becomes partially covered by a vapor film, decreasing the heat transfer. A local minimum heat transfer is reached once the plate is completely covered by vapor (point E in Figure 7). Afterwards, the heat flux starts again to increase with an increasing temperature as conduction through this vapor film increases with increasing temperature of the hot phase.

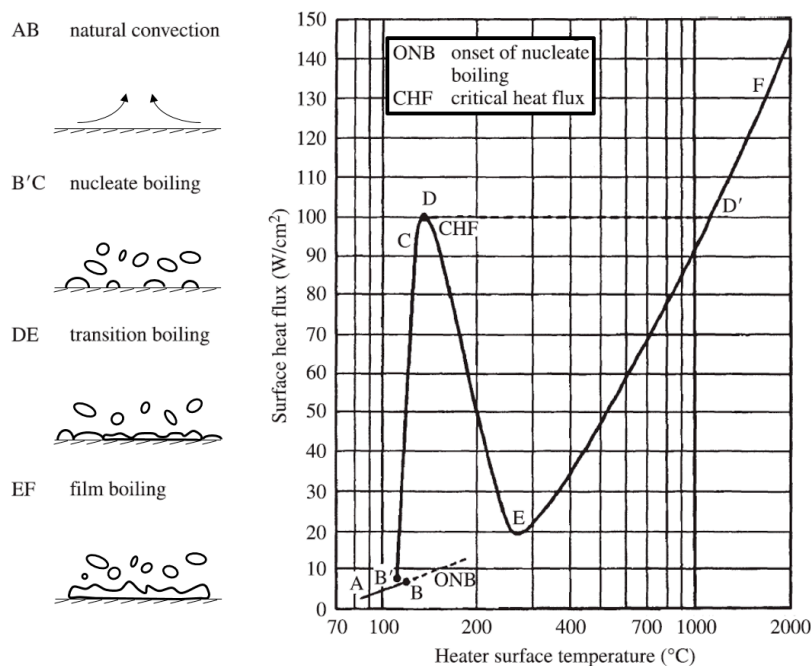


**Figure 7.** Heat flux (Y-axis) as a function of heater surface temperature (X-axis) showing the different boiling regimes for a horizontal plate submerged in a liquid (adapted from Reference [67]).

Whenever there is contact between a liquid pyrometallurgical phase and a coolant, the superheat is typically large enough for a vapor film to be present, and, hence, direct contact between the coolant and the hot phase is hindered. As such, the film boiling regime is the most important regime in the investigated system. Film boiling has been investigated in many different configurations, but the most relevant one in the context of this work is film boiling around spheres.

### 3.1. Early Descriptions of Film Boiling (at Boiling Temperature)

Bromley et al. [72,73] investigated heat transfer during film boiling and developed a theory based on the conductive and convective heat flow from a horizontal tube to the surrounding liquid, kept at boiling temperature. Radiation was also considered but was found to be negligible for standard ‘low-temperature’ applications. They assumed a dynamic equilibrium in which the heat going to the vapor film is used to continuously vaporize the liquid (heat entering the vapor film), while vapor was continuously leaving the interaction zone because of buoyancy or drag (heat leaving the vapor film). Part of the conducted heat was used to increase the temperature of the vapor layer, decreasing the heat flux towards the liquid. Further assumptions that were made included:

- Viscous flow, during which drag causes a certain velocity profile, is present (this assumption is based on visual evidence).
- The vapor layer is thin compared to the radius of the tube.
- A smooth interface is present between the vapor and the liquid.
- The film has constant thickness.
- The major part of the heat flux leaving the tube is used for evaporation, i.e., the vapor film has a very low heat capacity.
- Negligible kinetic energy is present in the vapor layer.

- It is permitted to use an average value for the temperature difference over the full vapor layer.
- All properties of the vapor film are measured at the boiling temperature.
- The vapor and the liquid are both incompressible.
- The sphere has a uniform temperature.
- Radiation can be neglected.
- Constant relative velocity of the droplet  $U_\infty$ .
- Constant evaporation rate per unit of area, independent of position around sphere.
- The system is symmetrical.

With these assumptions, their theory resulted in the following equation (obtained after numerical integration) for the heat transfer coefficient for convection ( $h_{conv}$ ) around a horizontal tube in a boiling liquid (Equation (9)).

$$h_{conv} \left[ \frac{D^2 \Delta T \mu_v}{U_\infty^2 k_v^3 \rho_v \rho_l \lambda'} \right]^{\frac{1}{4}} = 0.88 \left[ \frac{gD(\rho_l - \rho_v)}{4U_\infty^2 \rho_l} + \frac{3D\mu_v h_{conv}^2}{U_\infty k_v^2 \rho_l} \left( \frac{\pi}{\theta'} \right)^2 \right]^{\frac{1}{4}} \xrightarrow{U_\infty \gg 1} h_{conv} = 2.7 \sqrt{\frac{U_\infty k_v \rho_v \lambda'}{D \Delta T_{super}}}, \quad (9)$$

where  $k_v$  is the thermal conductivity coefficient of the vapor,  $\rho_i$  is the density of phase  $i$ ,  $g$  is the local acceleration of gravity,  $\lambda'$  is the difference in enthalpy between the vapor at its average temperature and the liquid at its boiling point,  $D$  is the outside diameter of the tube,  $\mu_v$  is the viscosity of the vapor,  $\theta'$  is the angle at which the vapor film detaches from the tube measured starting from the forward stagnation point, where the coolant 'splits' to pass the obstacle (see Figure 8),  $U_\infty$  is the relative velocity between the liquid coolant (bulk) and the hot phase, and  $\Delta T$  is the temperature difference between the tube and the boiling liquid. Equation (9) was derived from Bernoulli's theorem in the vapor film, and from the conservation of mass, momentum and energy between the phases. In the order of magnitude of the vapor film thickness, the coolant and the tube can locally be considered as two parallel plates. The boundary conditions are for laminar flow (no drag) between these parallel plates, one of which is moving (the water, seen from the moving sphere as frame of reference).

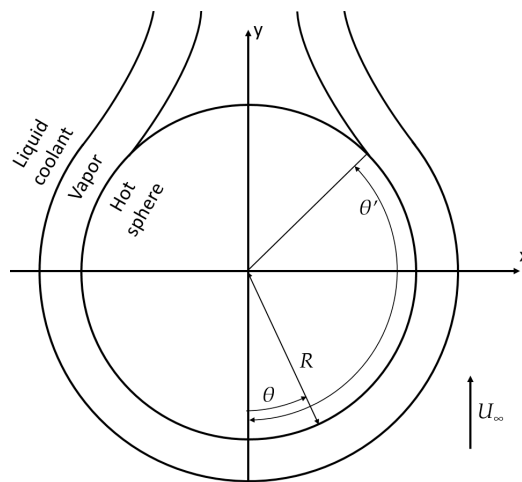


**Figure 8.** Schematic overview of a hot tube in a liquid coolant, showing the relative velocity  $U_\infty$ , the angular location variable  $\theta$ , the angle at which the vapor film detaches from the tube  $\theta'$ , and the radius of the droplet  $R$ .

Later, Kobayasi [74] used similar principles to find an equation for the heat transfer coefficient around a sphere during forced convection. In his paper, Kobayasi specifically mentions the relevance of this research for the solidification of a droplet of liquid metal falling through a coolant. In the derivation, he assumed axial symmetry. The only difference in the derivation was the shape: Kobayasi investigated heat transfer around a sphere,

whereas, for Bromley et al., it was around a tube. The study of Kobayasi resulted in the following equations:

$$h_{tot} = h_r + h_{conv} \quad (10)$$

$$h_r = \frac{\sigma_{sb}}{T_{hot} - T_l} \left( \epsilon_d \left( \frac{T_{hot}}{100} \right)^4 - \epsilon_l \left( \frac{T_l}{100} \right)^4 \right), \quad (11)$$

with  $h_{tot}$  the total heat transfer coefficient,  $h_r$  the heat transfer coefficient for radiation, and  $h_{conv}$  the heat transfer coefficient for convection. Here,  $h_r$  is calculated with Equation (11), where  $\sigma_{sb}$  is the Stefan-Boltzmann constant,  $T_i$  is the temperature of phase  $i$  (where 'hot' represents the hot sphere and 'l' the liquid coolant), and  $\epsilon_i$  is the emissivity factor of phase  $i$ . Caution should be taken when using this equation as to what value is implemented for  $\sigma_{sb}$ . Depending on the units, the factor 100 can be omitted [73,75,76]. In literature [67], one can find  $\sigma_{sb} = 5.667 \cdot 10^{-8} \text{ W/m}^2\text{K}^4$ , which is only valid without the factor 100. The factor 100 can be inserted in the equation (as in Equation (11)) if one uses  $\sigma_{sb} = 5.667 \text{ W/m}^2\text{K}^4$ . The factor 100 was left in Equation (11), but the correct value and units for  $\sigma_{sb}$  (see Nomenclature) were used.

The heat transfer coefficient for convection is less trivial to determine. Like Bromley et al. [73], Kobayashi [74] also had to calculate the results of his equation numerically. The obtained numerically-fitted equation is presented in Figure 9 for different Prandtl numbers, where  $Nu$ ,  $Pr$ ,  $Re$ ,  $R$ ,  $\nu_l$  represent the Nusselt, Prandtl, and Reynolds numbers, the radius of the sphere, and the kinematic viscosity of the liquid, respectively. From these figures, it is possible to determine the Nusselt number (and thus the heat transfer coefficient) if one knows the other properties of the liquid, the vapor, and the flow.

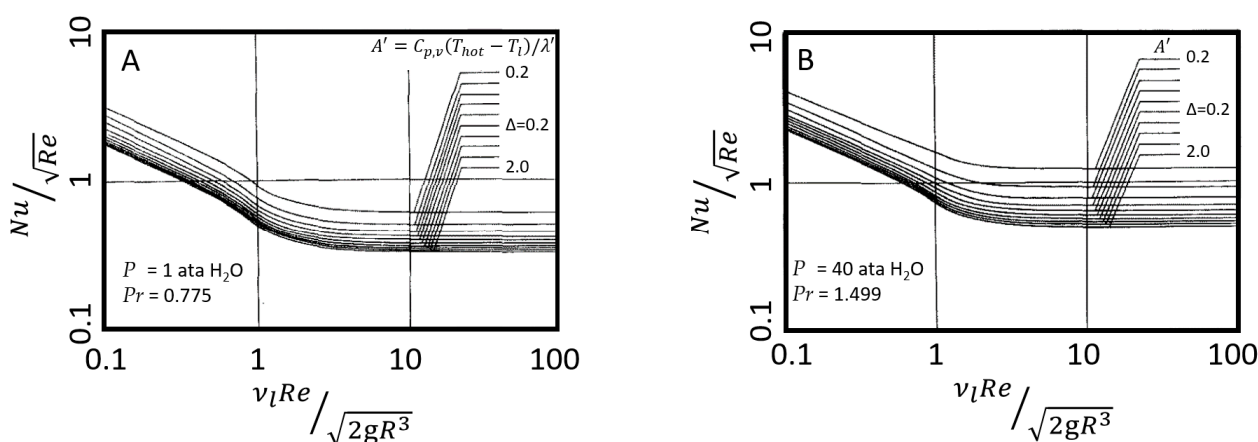


**Figure 9.** Ratio of Nusselt ( $Nu$ ) number and square root of Reynolds ( $Re$ ) number  $Nu/\sqrt{Re}$  in water with forced convection film boiling (Y-axis) as a function of sphere size ( $R$ ) and relative velocity ( $v_l$ , X-axis) for a variation in energy content  $A' = C_{p,v}(T_{hot}-T_l)/\lambda'$  at different external conditions (adapted from Reference [74]): (A) 1 ata  $H_2O$ ; (B) 40 ata  $H_2O$  (ata is an old pressure unit for the total pressure (hydrostatic + atmospheric)).

Witte [77] also investigated film boiling around a sphere in a flowing and saturated (i.e., at boiling temperature) liquid. In his theoretical investigation, he made the assumption that the liquid velocity at the interface can be calculated from potential flow theory, which resulted in an equation with less variables that can be solved analytically. The investigation started from the energy-mass balance at the interface between the vapor and the liquid, assuming that little energy is used for heating the vapor. Even though the configuration and the assumptions were different (Bromley studied forced convection around a tube, while Witte studied forced convection around a sphere using the potential flow theory),

the numerically-fitted equation found by Bromley (Equation (9)) is very similar to the analytical equation found by Witte (Equation (12)).

$$h_{conv} = \sqrt{\frac{\rho_v \lambda' U_{\infty} k_v}{8R\Delta T}} \int_0^{\pi} \frac{\sin 3(\theta)}{\int_0^{\theta} 2\sin 3(\theta') d\theta'} d\theta = 0.465 \sqrt{\frac{\rho_v \lambda' U_{\infty} k_v}{D\Delta T_{super}}} \quad (12)$$

### 3.2. Influence of Subcooling of the Liquid on Boiling Behavior

The models discussed in Section 3.1 are limited to cases where the coolant is at its boiling temperature. When the coolant is not at its boiling temperature, part of the heat is transferred from the hot phase to the liquid coolant, hence creating a temperature gradient inside the liquid coolant, going from its boiling temperature to its bulk temperature. In most practical cases, the coolant has a temperature below its boiling temperature. In this work, the amount of subcooling represents the difference between the coolant bulk temperature and its boiling temperature. In other words, the coolant subcooling should be included in the models to describe reality better.

The influence of the subcooling has been investigated theoretically by Sparrow and Cess [78] and Nishikawa and Ito [79]. These studies are similar to the studies above and mainly show predicted dependencies, which will be discussed in Section 3.6. They differ from the above discussed studies by the fact that they solve a two-phase boundary-layer problem. The problem was solved by using the differential equation of the conservation of mass, momentum, and energy in both boundary-layers. The only difference between the results of Sparrow and Cess [78] and Nishikawa and Ito [79] originates in their assumptions. The first included three assumptions for these equations and the conditions at the interface, whereas Nishikawa and Ito did not agree with the third assumption:

- Viscous dissipation can be neglected due to low velocities (effect on energy conservation).
- Linear temperature profile in vapor film is only in limiting case.
- Flow induced by the shear forces at the interface can be neglected as compared to free convection in both the liquid and the vapor (effect on boundary conditions at the interface)

On the other hand, this influence was also investigated experimentally. One of the first experimental studies on heat transfer in natural convection was performed by Bradfield [80]. In his experiments, he measured the cooling rate of his sample, which showed clear deviations as the boiling regime changes during cooling (see Figure 10A). Even though the figure does not have SI-units, it is clear that, whenever the liquid has higher subcooling (i.e., a lower liquid temperature  $T_l$ ), the onset of film boiling was shifted to higher sphere temperatures, thus having a higher wall temperature  $T_{hot}$ . Both the maximum heat flux during nucleate boiling (indicated as 'X' on Figure 10A for  $T_l = 27^\circ\text{C}$ ) and the minimum heat flux during film boiling (indicated as '\*' on Figure 10A for  $T_l = 27^\circ\text{C}$ ) also increased with decreasing  $T_l$ . If one takes the combination of coolant bulk temperature and the temperature of the corresponding point 'X' and puts it in a plot, it is found that this shift in the onset of film boiling is approximately linear with the subcooling of the liquid (see Figure 10B).

### 3.3. Influence of Relative Movement of Phases on Boiling Behavior

Stevens and Witte [81] performed an experimental study to investigate the influence of both subcooling and relative velocity between hot and cold phases on the transition from film to nucleate boiling (the regime in between is referred to as the transition boiling regime, see Figure 7). They found that the temperature at which transition starts (i.e., the transition temperature ( $T_{trans}$ ), when the first visual proof of destabilization of the vapor film was observed) is independent of the relative velocity between the two phases (in the investigated range) but increases with increasing initial sphere temperature  $T_{ini}$  (Figure 11A). Furthermore, they also observed that heat transfer increases with increasing

relative velocity and increasing  $T_{ini}$  (Figure 11B). Lastly, they observed that  $T_{trans}$  increased with increasing water temperature (grey/black in the same image), which is opposite of what was found before by Bradfield [80]. The results of Stevens and Witte (originally Figure 4 a and b in Reference [81]) later turned out to be erroneous, as the grey line should be above the black line in Figure 11A.

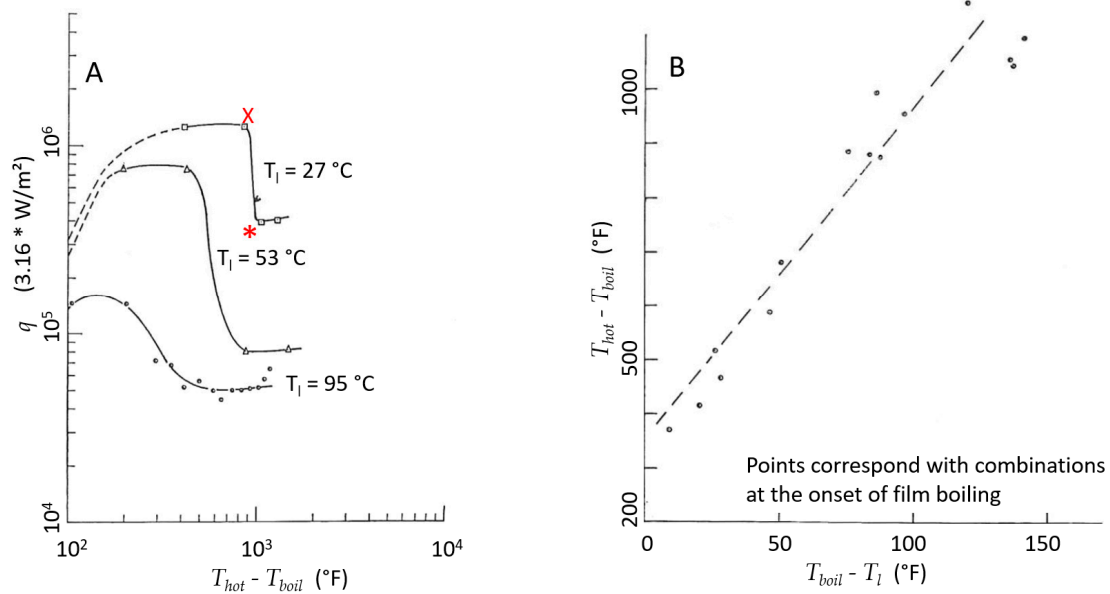


**Figure 10.** Dependency of boiling curve on subcooling of liquid (adapted from Reference [80]): (A): the ratio of heat flux and surface area ( $q/A$ ) versus hot phase temperature ( $T_{hot}$ ) for different values of coolant temperature ( $T_l$ ); (B): ( $T_{hot} - T_{boil}$ ) versus ( $T_{boil} - T_l$ ) at the onset of film boiling (where  $T_{boil}$  is the boiling temperature).

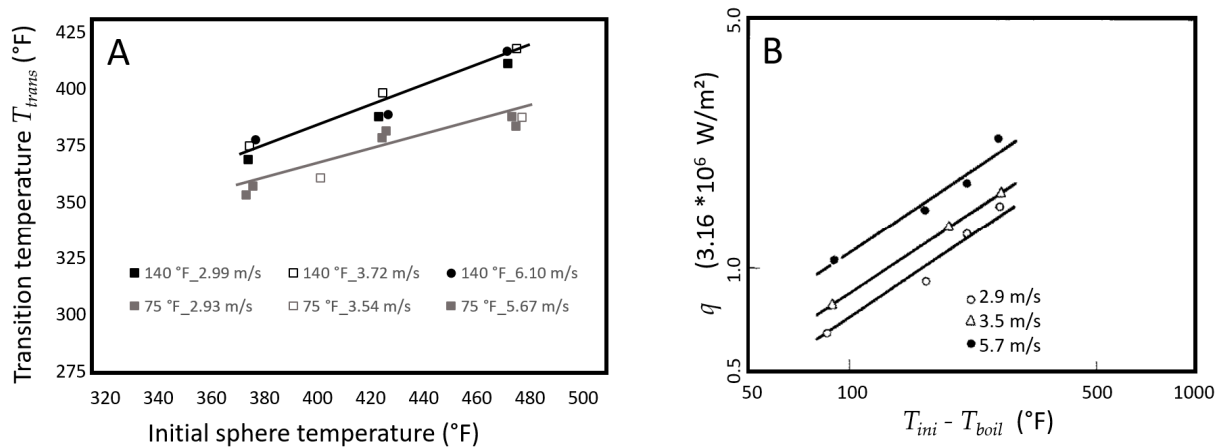


**Figure 11.** Effect of initial temperature ( $T_{ini}$ , X-axis) in transition boiling regime around a sphere (adapted from Reference [81]): (A) Transition temperature ( $T_{trans}$ , Y-axis) for different relative velocity ( $\bullet/\square/\blacksquare$ ) and coolant temperature  $T_l$  (grey/black; this trend later turned out to be erroneous); (B): The heat flux ( $q$ , Y-axis) for different relative velocities.

From Figure 11, the following conclusions can be drawn:

- a) Increasing the relative velocity ( $U_\infty$ ) between both phases increases the heat leaving the sphere ( $J/(kg_{hot} \cdot s)$ ) without changing  $T_{trans}$ . Because of the higher  $U_\infty$ , the mass of water passing the hot phase rises ( $kg_l/(s \cdot kg_{hot})$ ). The ratio of these quantities is the energy being absorbed by the coolant ( $J/kg_l$ ). Since both quantities increase with an increasing  $U_\infty$ , the change in this ratio is minor, i.e., the energy transfer to the water

remains rather constant. This suggests that the transition is determined by a critical heat flux ( $q_{trans}$ ), which will be discussed later in this section.

- b) Increasing the water temperature  $T_l$  is expected to decrease the heat flux ( $q$ ) to the water because the driving force (i.e., the temperature difference or gradient) reduces. The influence of  $T_l$  on  $q$  was not investigated experimentally in this study. On the contrary, the influence of  $T_l$  on  $T_{trans}$  was investigated and seemed to result in a higher transition temperature (Figure 11A). However, this observation was later proven erroneous.
- c) The increased  $T_{trans}$  for increased  $T_{ini}$  could indicate a kinetic effect on the destabilization of the vapor film. Keeping in mind a possible  $q_{trans}$  suggested in conclusion a), an explanation could be that a higher  $T_{ini}$  results in a thicker vapor film, which needs a higher  $\Delta T$  to sustain  $q_{trans}$  (see Equation (13)). The reader is reminded that the influence of  $T_{ini}$  was one of the uncertainties of the studies discussed in Section 2. It turns out that this influence has been studied before in case of a solid hot phase (cfr. this study by Stevens and Witte [81]). However, later studies never investigated the influence of  $T_{ini}$ , even though a lot of open questions remained.

$$q_{trans} = h_{trans} \cdot (T_{trans} - T_l) = k_v \cdot \frac{(T_{trans} - T_l)}{\delta_{trans}}. \quad (13)$$

A later study by Stevens and Witte [66] also included a characterization of the vapor layer destabilization (Figure 12A). The transition from film to nucleate boiling occurs in multiple steps:

1. First, the initial vapor film becomes unstable, either progressively or suddenly (i.e., with a transplosion). The name ‘transplosion’ was first mentioned by Stevens and Witte [82] and was used to describe the very rapid physical interaction caused by the submergence of a hot phase into a volatile coolant. They saw that the explosive transition from film boiling to pulsation boiling occurred within 1 frame of the high-speed video (less than 0.25 ms).
2. The second step is pulsation boiling, during which the prior stable vapor film is continuously pulsating perpendicular to the sphere surface (either homogeneously or heterogeneously), as can be seen by the small arrow in Figure 12B.
3. The final step is the movement of the region with pulsation boiling. This region is sweeping over the surface of the sphere as a ring, resulting in a progressive transition from film boiling to nucleate boiling. At this moment, both nucleate boiling and film boiling are observed with a transition zone, i.e., a pulsating vapor ring, in between. That is why this step in the transition is referred to as 3-region boiling (see Figure 12B).

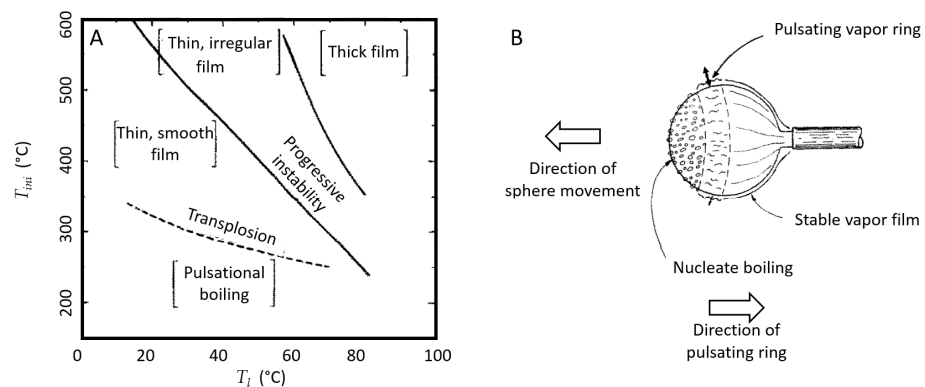


**Figure 12.** Additional findings of Stevens and Witte (adapted from Reference [66]): (A) Characterization of vapor film (and its destabilization, i.e., step 1) as a function of coolant temperature ( $T_l$ , X-axis) and initial sphere temperature ( $T_{ini}$ , Y-axis); (B) graphic representation of 3-region boiling (i.e., step 3).

A little more explanation is required on the destabilization of the vapor shell (above-mentioned step 1). They observed that destabilization of a thin and smooth film (i.e., precipitous instability via transplosion) happened rapidly, whereas it was slower for a thin and irregular film (i.e., progressive instability), while a thick film did not destabilize at all during its passing through the water tank. The difference between these observations is discussed in more detail below:

a) A transplosion (both  $T_l$  and  $T_{ini}$  are relatively low; cfr. Figure 12).

A rapid change in boiling mode over the entire vapor shell, without any visible indication. In these experiments, a transplosion was observed around a solid. In later research, Zyszkowski [47] observed this phenomenon around solidified debris in his experiments with molten copper (see Section 2.2).

b) A progressive instability (both  $T_l$  and  $T_{ini}$  have an intermediate value; cfr. Figure 12).

Starts from a stable film with bubble-like irregularities and is defined by the movement, growth and collapse of these irregularities. This triggers oscillations in the vapor film perpendicular to the sphere surface, which then gradually spread over the sphere surface.

c) A thick and stable vapor layer (both  $T_l$  and  $T_{ini}$  are relatively high; cfr. Figure 12).

No sign of any destabilization, probably because the maximum decrease in temperature in the duration of the experiment was not sufficient to destabilize the vapor film.

From the described observations, we obtain the hypothesis that precipitous destabilization occurs via homogeneous nucleation (many random nucleation sites lead to fast transition), whereas progressive destabilization occurs via heterogeneous nucleation (slow transition due to a smaller number of effective nucleation sites). The reason for this hypothesis is the fact that progressive instability shows more possible nucleation spots. Furthermore, a progressive instability might occur at higher temperatures, inhibiting the homogeneous nucleation of liquid water. However, only the initial temperature was monitored during the experiment; hence, there is no record of the interface temperature at the moment of the instability/transplosion; therefore, this remains uncertain. But, the hypothesis can be endorsed by Figure 11A, where it was seen that  $T_{trans}$  increases as  $T_{ini}$  increases.

The second observation of Stevens and Witte was that a critical parameter for film boiling stability is the heat flux leaving the hot phase (cfr. the constant heat flux at the moment of transplosion in Figure 13) rather than the temperature of the sphere (cfr. varying  $T_{trans}$  in Figure 11A). It was found that there exists a critical heat flux to sustain film boiling, which was also suggested above. This critical heat flux decreases with increasing water temperature  $T_l$  (squares vs. circles in Figure 13), probably because warmer water needs less energy to vaporize. A decreased critical heat flux also explains the lower  $T_{trans}$  for higher  $T_l$  (cfr. Figure 10B). From these observations, we obtain the hypothesis that the critical heat flux will also be a function of the relative velocity between the two phases. We assume that the critical heat flux per unit mass leaving the hot phase ( $J/(kg_{hot}\cdot s)$ ) is determined by the product of a constant (only dependent on coolant temperature, see Figure 13) critical energy entering the water ( $J/kg_l$ ) and the amount of water passing the hot phase per unit of time ( $kg_l/(kg_{hot}\cdot s)$ ). Here, the reader is reminded that the considered configuration is that of a relatively small droplet of molten pyrometallurgical phase dropped into a relatively large amount of coolant (see Section 1).

The idea of a critical heat flux can also be used to explain some of the observations in Section 2. For example, if a higher initial temperature  $T_{ini}$  is used, this might result in a higher thickness of the vapor layer ( $\delta$ ). Since this vapor layer acts as an insulation for heat transfer, the heat flux will be a function of both the temperature difference and  $\delta$ . If the temperature of the hot phase  $T_{hot}$  is changing more rapidly than  $\delta$ , then there will be no equilibrium between  $T_{hot}$  and  $\delta$ . As such,  $\delta$  could have different values for constant  $T_{hot}$ , depending on  $T_{ini}$ . An increase in  $\delta$  with increasing  $T_{ini}$  explains both the increase in  $T_{trans}$  observed in Figure 11A and the decrease in 'distance to explosive site' in Figure 3B. Lastly, it also explains why one should not use the instantaneous temperatures in Figure 4.

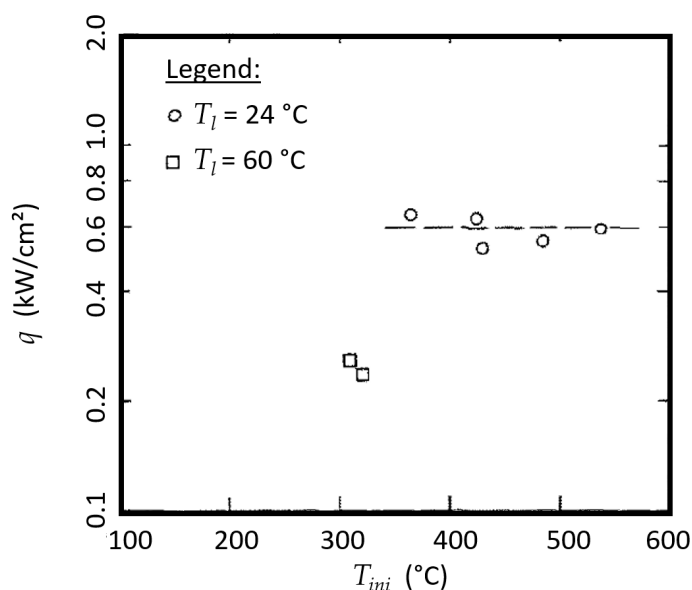


**Figure 13.** Heat flux at the moment of transposition ( $q$ , Y-axis) as a function of the initial sphere temperature ( $T_{ini}$ , X-axis) for different coolant temperatures (adapted from Reference [66]).

Another investigation regarding film boiling during both natural and forced convection in both subcooled and saturated water around a sphere was performed by Dhir and Purohit [83]. For the case of natural convection, they performed a theoretical derivation of the equation for  $Nu$  (or heat transfer coefficient, similar to theoretical studies discussed above). Next, the heat transfer coefficient around spheres (diameter: 19 mm and 25.4 mm; material: steel, copper and silver) in water was experimentally studied both in natural and forced convection.

In their theoretical analysis, Dhir and Purohit included the solid hot sphere, a vapor layer, a hydrodynamic and thermal boundary layer, and the non-affected surrounding water. The sphere was held at a constant position and the vapor and water within the boundary layer were moving upward by natural convection. They used the same method as both Sparrow and Cess [78] and Nishikawa and Ito [79], namely they started from the differential form of the conservation laws. The difference lays in the assumptions that were made:

- A uniform and constant sphere temperature, resulting from an internal heat source.
- The vapor layer is relatively thin as compared to the sphere radius, implying a linear temperature profile in the film and negligible inertia of the film.
- The hydrodynamic and the thermal boundary layer have the same thickness.
- There is no slip between the vapor layer and the boundary layer.

The analysis resulted in some complex equations, which need to be solved implicitly (the reader is referred to the work of Dhir and Purohit [83] for more details). Besides some material properties and geometrical conditions, the equations also have two dimensionless numbers,  $Sh$  and  $Sc$ , which can be seen in Equations (14) and (15). They represent the superheating of the melt (difference between  $T_{hot}$  and the boiling point of the coolant) and the subcooling of the coolant (difference between  $T_l$  and the boiling point of the coolant), respectively. The results of the model are incorporated in Table 2 and further discussed in Sections 3.4 and 3.5.

$$Sh = \frac{C_{p,v}\Delta T_{super}}{\lambda'} \quad (14)$$

$$Sc = \frac{C_{p,v}\Delta T_{sub}}{\lambda'} \quad (15)$$

**Table 2.** Overview of the used influence parameters in the different models for  $Nu$  (Dhir and Purohit; M and E refers to their theoretical model and empirical relation, respectively); clear: not considered in model, grey arrow: considered as a combination of multiple parameters, black arrow: considered by itself; arrows show the effect on  $Nu$  (up = positive correlation, down = negative correlation; only when present in final results (figures/formulas)); ? refers to the assumed typographical error in the formulas for the empirical relation obtained by Dhir and Purohit [83].

| $Nu \uparrow$ ( $T_{trans} \downarrow, \delta_{trans} \downarrow$ ) | Sparrow and Cess (1962)                                 | Nishikawa and Ito (1965)                             | Dhir and Purohit M (1978)                                  | Dhir and Purohit E (1978) | Bromley (1953)                 | Kobayasi (1965)                  | Witte (1968)  |
|---|---|--|--|---------------------------|--------------------------------|----------------------------------|---|
| Energy transfer vapor ( $Pr_v$ )                                    |   | ↑  |  | ↑                         | ↑                              | ↑                                | ↑   |
| Superheating ( $Sh$ )   | ↓   | ↓  | ↓  | ↓                         | ↓                              | ↓                                | ↓   |
| Subcooling ( $Sc$ )   | ↑   | ↑  | ↑  | ↑                         |                                |                                  |   |
| Energy transfer liquid ( $Pr_l$ )                                   | ↓   | ↓  |  | ↓                         |                                |                                  |   |
| Liquid thermal expansion ( $\frac{C_{p,l}}{\beta\lambda}$ )         | ↓   | ↓  |  | ?                         |                                |                                  |   |
| $\mu$ -ratio ( $\frac{\mu_v}{\mu_l}$ ) <sup>2</sup>                 | ↓   | ↓  |  | ↓                         |                                |                                  |   |
| $\rho$ -ratio ( $\frac{\rho_v}{\rho_l}$ )                           | ↓   | ↓  |  | ?                         |                                |                                  |   |
| Archimedes force ( $Ar$ )   | ↑   | ↑  | ↑  | ↑                         | ↑                              | ???                              |   |
| Fluid velocity ( $Re$ )   |   |  |  | ↑                         | ↑                              | ↑                                | ↑   |
| Methodology   | two-phase boundary-layer, vertical plate, without shear | two-phase boundary-layer, vertical plate, with shear | two-phase boundary-layer, sphere, without inertia of vapor | empirical                 | one-phase boundary-layer, tube | one-phase boundary-layer, sphere | one-phase boundary-layer, sphere, potential flow theory |

Dhir and Purohit [83] did not include forced convection in their model. However, they did study the influence of the relative velocity between both phases experimentally (see Figure 14). It was seen that the transition temperature would increase if the water temperature is decreased, but that the relative velocity showed virtually no influence on the transition temperature. The latter has also been found experimentally by Bradfield [80] (Figure 10B) and by Stevens and Witte [81] (Figure 11A).

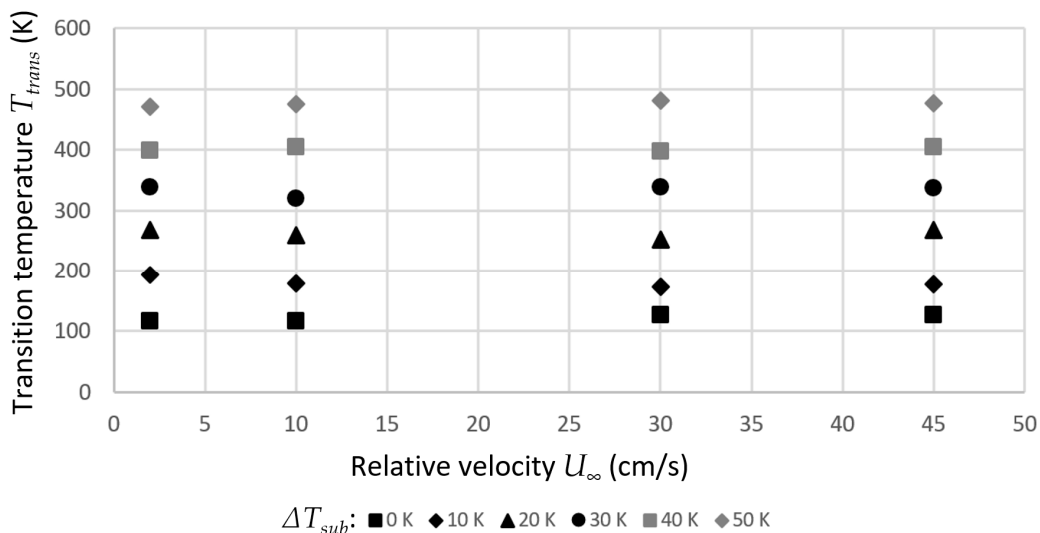


**Figure 14.** Experimental data for the influence of the relative velocity ( $U_\infty$ , X-axis) on the transition temperature ( $T_{trans}$ , Y-axis) at different subcoolings of the coolant (different symbols in graph) (graph created from numerical values in Reference [83]).

3.4. Influence of Material Properties on Boiling Behavior

Dhir and Purohit [83] noticed that the thermophysical properties of the sphere had no effect on the transition temperature during experiments as long as the surface was smooth and clean (data points in Figure 15), even though this was suggested otherwise by Henry in a theoretical study [84] (lines in Figure 15) and is also suggested by Equations (3) and (4). The experimental results of Dhir and Purohit even contradicted their own theory. Furthermore, Dhir and Purohit found an empirical relation for the minimum superheating of the hot phase corresponding with a certain coolant subcooling to obtain film boiling (Equation (16)). Note the similarity between Equation (7) (theoretically approximated) and Equation (16) (empirically determined). Furthermore, Equation (16) shows a linear dependency between  $T_{MFB}$  and  $T_l$ , which was also seen in the theoretically derived Equations (3) and (4).

$$\Delta T_{MFB} = 101 + 8\Delta T_{sub}. \tag{16}$$

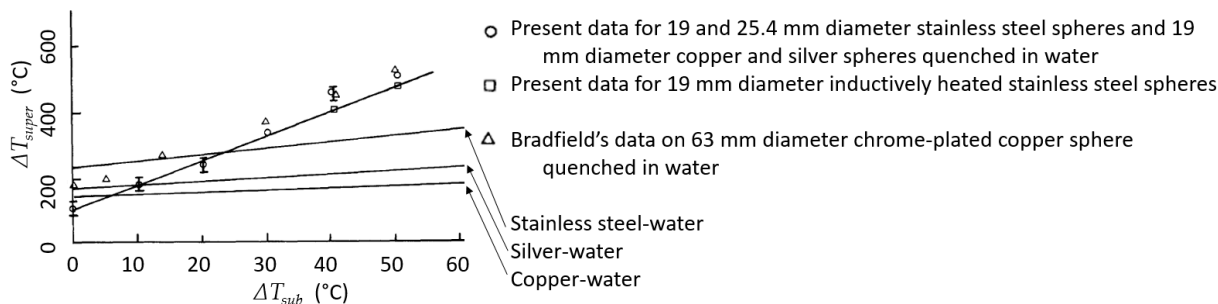


**Figure 15.** Minimum film boiling temperature for a combination of coolant subcooling ( $\Delta T_{sub}$ , X-axis) and hot sphere superheating ( $\Delta T_{super}$ , Y-axis): experimental (data points connected by a single line) versus theoretical (three separate lines less inclined without data points) (adapted from Reference [83]).

In their experiments, Dhir and Purohit [83] also measured the heat transfer coefficient (data points in Figure 16) and compared it to their theoretical model (represented by the dash-dotted lines in Figure 16). It can be seen that the model predicts the same trends as the experiments, but that the predictions are 25–40% lower. Initially, the heat transfer coefficient increases with decreasing water temperature (corresponding to a higher subcooling and, hence, a higher  $Sc$  number), but this increase ends in an asymptotic manner. The results have been represented by an empirical relation (Equation (35) in Figure 16; thus, as in Reference [83]), but we assume there is a typographical error in this equation since the units do not match (Equation (37) in Reference [83]). As there is some uncertainty about this equation, we did not include it in this review paper.

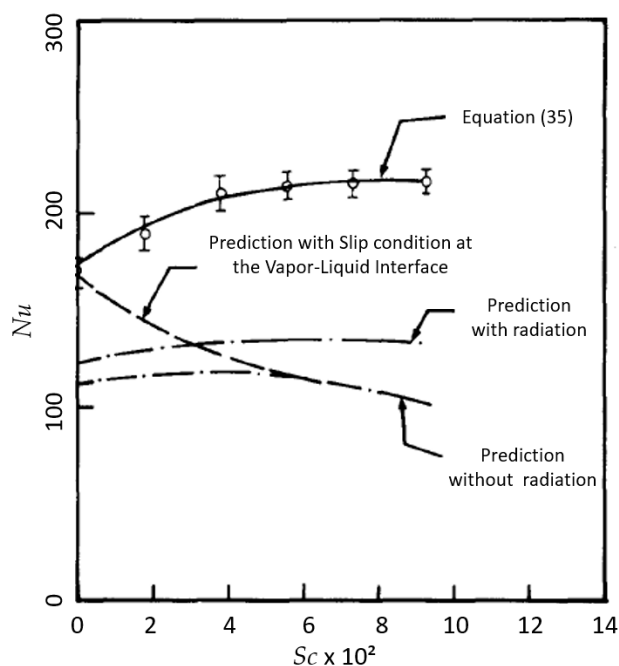


**Figure 16.** Data and models for natural convection heat transfer (represented by  $Nu$  (Y-axis)) as a function of the coolant subcooling (represented by  $Sc$  (X-axis)) for 19-mm diameter Cu, Ag, and stainless steel spheres (adapted from Reference [83]).

### 3.5. Influence of the Size of the Material on Boiling Behavior

The abovementioned empirical equation (Equation (35) in Figure 16 and in Reference [83]) includes both convection and radiation, where radiation only accounts for 10% of the energy transferred in these experiments. Focusing on the terms for convection, it was observed that the Nusselt number varies with the diameter ( $D$ ) as  $D^{3/4}$ . The dependence of the heat transfer coefficient on the size of the sphere was proven with another experiment by Dhir and Purohit [83] using a 25.4 mm diameter stainless steel sphere, confirming that the heat transfer coefficient varies with  $D^{-1/4}$  ( $Nu$  varies with  $D^{3/4}$ ). Furthermore, it was found that their model (dash-dotted line in Figure 16) is an underestimation of the heat transfer. The authors gave three possible explanations for the difference:

1. Underestimation of the interfacial surface area due to small capillary waves.
2. Overestimation of the thickness of the boundary layers due to small capillary waves.
3. Underestimated amount of liquid sucked from the convective boundary layer, thereby thinning the vapor film.

### 3.6. Comparison of Previous Results

A final series of experiments was performed to investigate the influence of the relative velocity between the sphere and the water on the heat transfer coefficient. First, the experiments were performed with water at its boiling point (Figure 17A). The figure also

shows some relations determined by other researchers that were discussed above (e.g., the curve referred to as ‘Bromley [73] for cylinders’ represents Equation (9)). Dhir and Purohit mention that Witte did not take buoyancy into account, which could explain the difference. Witte himself mentioned that he expected this formula to be an underestimation by a factor of 4.25. He found this factor 4.25 based on the comparison of his theoretical derivation with experimental results, both for forced convection in saturated water around horizontal cylinders. He had no immediate physical explanation for this factor but assumed that it would also be applicable for the derivation for spheres. This factor 4.25 would bring the curve much closer to the experimental values.

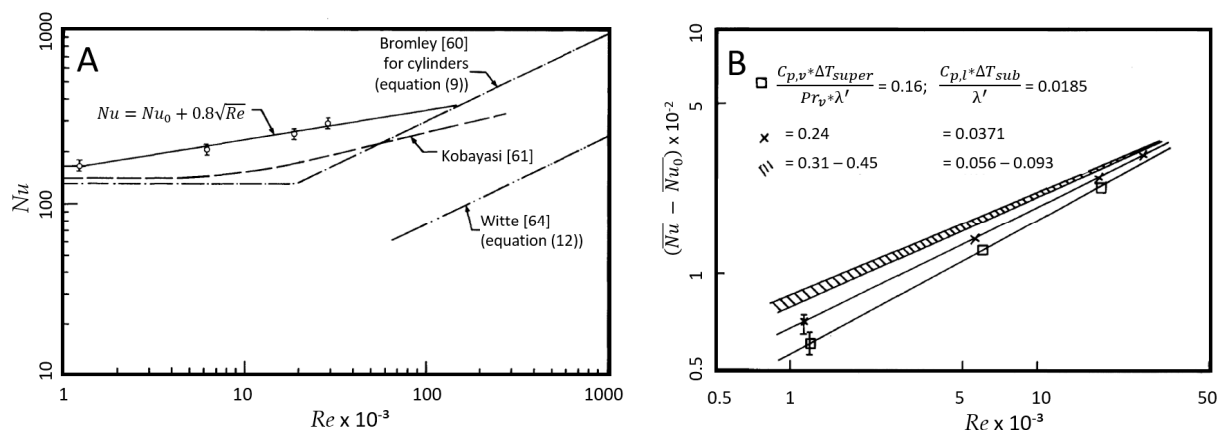


**Figure 17.** Heat transfer coefficient (represented by Nusselt number (Y-axis)) during forced convection around a 19-mm stainless steel sphere as a function of relative velocity (represented by Reynold number (X-axis)) for different sphere and coolant temperatures (adapted from Reference [83]): (A) Saturated water; (B) subcooled water.

Afterwards, the combination of subcooling ( $\Delta T_{sub}$ ) and relative velocity (represented by  $Re$ ) was investigated (see Figure 17B). The increase in  $Nu$  by decreasing the water temperature is observed in this representation, as well, also showing the diminishing influence of subcooling. Furthermore, it is expected that the effect of the subcooling will be negligible as compared to the forced convection effect. Finally, Equation (17) was found as an empirical relation including both  $\Delta T_{sub}$  (represented as  $Sc$ ) and  $Re$  for forced convection. The main difference between the empirical relation from Figure 16 and Equation (17) is that the latter neglects radiation and thermal expansion. The influence of the subcooling is implemented similarly in both equations.

$$\overline{Nu} = \overline{Nu}_0 + 0.8\sqrt{Re} \left( 1 + \frac{Sc Pr_v \mu_l}{Sh Pr_l \mu_v} \right). \quad (17)$$

It was seen that these equations for natural convection around a sphere are dependent on a total of 9 variables. The equations of Sparrow and Cess [78] for natural convection only had 5 variables. Nishikawa and Ito added a 6th variable for the case of natural convection, whereas Kobayasi [74] named 4 variables for the case of forced convection.

This variation in the number of used influencing parameters has been visualized in Table 2. In this table, grey indicates that the model uses a combination of multiple parameters that are related to each other but are independent in other models (e.g., Sparrow and Cess [78] combine the ‘liquid thermal expansion’, the ‘viscosity ratio’, and the ‘density ratio’ into one variable, whereas Dhir and Purohit [83] consider these as three different variables). Furthermore, it was attempted to show the influence of the different parameters. However, this was not straightforward as most of these models are numerical which implies that the influences need to be obtained from the resulting graphs. Even more, some authors did not include the influence of every variable in their graphs. Even though they considered the variables in the derivation, they did not include the influence of that

particular variable in the published results. This is visualized in Table 2 as an empty black cell.

From Table 2, it can be seen that the model of Dhir and Purohit [83] (see ‘Dhir and Purohit M. (1978)’) uses almost all parameters that were used by any of the other discussed models, showing the progress that has been made over the years. On the other hand, they also provided an empirical model (see ‘Dhir & Purohit E. (1978)’) showing many of the same parameters in the tested range. It should be noted that a problem arose because of the assumed typographical error in their paper, making it impossible to determine the influence of the ‘liquid thermal expansion’ and of the ‘density ratio’ (represented by a question mark in a black cell). Finally, the models of Bromley [73], Kobayasi [74] and Witte [77] have been added to the right-most columns, since these consider forced convection. For these cases, Witte intentionally included less variables in order to make an analytical solution possible. The reason for the uncertainty about the influence of the ‘Archimedes force’ in the model of Kobayasi is that he did not exactly use a dimensionless number on the X-axis in his graphs (see Figures 3–5 in Reference [74]). Taking into account the suspected critical heat flux  $q_{trans}$ , it can be concluded that an increasing  $Nu$  (for constant geometry, conductivity of the vapor, and critical heat flux of the coolant) causes an increased heat transfer coefficient, which will result in a decreased transition temperature  $T_{trans}$ , and decreased film thickness  $\delta_{trans}$  (see Equation (13)).

Many of the above-cited authors mention the relevance of research regarding boiling regimes in the investigation of vapor explosions. Dhir and Purohit [83] even had a section in their paper called ‘An application to fuel-coolant thermal interactions’. This proves that it has been thought for a long time that heat transfer will play a major role in the phenomenon of vapor explosions, demonstrating the relevance of the above section. Unfortunately, recent studies regarding heat transfer during film boiling have not been able to explain the abovementioned problems. One of these more recent studies is the investigation by Jouhara and Axcell [85] in 2009. They performed an experimental study in which they mainly had similar observations as were made before by other researchers like Stevens and Witte [66]. The main difference in the experimental part was possibly because of the improved technology, making new observations possible. This proves the relevance of repeating experiments, as long as one remembers former studies, which was nicely demonstrated by Jouhara and Axcell [85]. Besides their experimental work, they also tried to model heat transfer around a vertical plate. Their model showed a discrepancy of about 10%, which could increase with increasing plate dimensions. This proves that heat transfer is still not completely understood today. The next section further shows the relevance of understanding on heat transfer in the implementation and development of contemporary models for vapor explosions.

#### 4. Modeling Vapor Explosions

In Section 3, some steady-state models (implying a heat source inside the droplet) for heat transfer were described. Dhir and Purohit [83] stated that these models can be interesting in case the time constant for heat transfer is large relative to the time constant for the dynamics of the vapor film (i.e., a quasi-static temperature profile while the thickness of the vapor film is changing). However, they do not prove the validity of this assumption. Furthermore, the reader is referred to Section 2.3, where the temperature interaction zone (TIZ) was discussed. There, it was said that no explosion would occur if the initial conditions are outside of the TIZ, even if the instantaneous combination of temperatures passed through this zone, probably due to the dynamics of the vapor layer. In other words, the temperature of both phases is expected to change more rapidly than the thickness of the vapor layer and as such, no quasi-steady-state is expected. This idea is supported by the fact that  $T_{trans}$  is a function of  $T_{ini}$ , suggesting that vapor film dynamics are slower than heat transfer dynamics. Hsiao et al. [52] said that the vapor film in the film boiling regime is not in steady-state, but that both the temperature field and the vapor film are

in an unsteady-state. Further research is definitely needed on this subject, showing the importance of transient models.

However, steady-state models are also interesting as they can be used to make rough predictions about the heat transfer, which can be related to the TIZ. Matsumura and Nariai [86] used this method and they found that the shape of the TIZ depended on the heat transfer coefficient  $h$ , which was expected as the  $T_{MFB}$  depends on  $h$ , as well. Their results qualitatively agree well with the TIZ obtained by Dullforce et al. [53], which was represented in Figure 4.

More recent models include parametric and transient models. Parametric models are of high value for industry but are of lesser importance for fundamental research. These models are often capable of predicting whether a vapor explosion will occur, but they cannot say why it occurs or how it can be prevented. Transient models are better for fundamental research but they might require a lot of computational power on industrial scale. In this review paper, only transient models will be further discussed. More information about parametric models can be found in Reference [9,10,23].

Further research regarding the various steps during a vapor explosion was performed by Hsiao et al. [52]. They developed an analytical model for the occurring events after impingement of a hot molten drop into a volatile coolant, including vapor film collapse and droplet fragmentation. They specifically included the idea that the vapor film collapses locally rather than homogeneously. Because of heterogeneous collapsing, the moving coolant might form a protrusion [87], which could penetrate the droplet and cause fragmentation according to Board et al. [88]. Using data available at that time regarding heat flux from a submerged nickel foil in water ( $9.148 \times 10^7 \text{ W/m}^2$  [89]), typical duration of collapse of the vapor film around the same nickel foil ( $30 \mu\text{s}$  [89]) and limit-of-superheat temperature (i.e.,  $T_{HN}$ ,  $269 \text{ }^\circ\text{C}$  [90]), Hsiao et al. [52] were able to estimate the volume change due to evaporation. This volume change happens so rapidly during the cyclic growth and collapse of the vapor film that it is sometimes referred to as flashing [52] of the superheated coolant. The used data resulted in a layer with a thickness of  $0.4 \mu\text{m}$  in which the coolant reached  $T_{HN}$ . Evaporation of this layer results in a vapor layer of a few hundred micrometers, which corresponds well with experimental measurements by Stevens et al. ( $250 \mu\text{m}$  [82]). The volume change resulting from the evaporation of this layer ( $0.4 \mu\text{m}$  expands to  $250 \mu\text{m}$ ) is very small and cannot be responsible for the vapor explosions according to Hsiao et al. [52]. As such, flashing must be followed by an additional heat transfer and corresponding volume change. The question remains whether this energy is sufficient to cause fragmentation.

Since transient models include time, they usually consist of differential equations. The reader is referred to the work of Hsiao et al. [52] for the explicit development of equations on fragmentation and on the transient vapor film thickness. Only the main conclusions are mentioned here. For example, equations for the motion of the droplet in air and the impingement with water do not show any indication for fragmentation. Furthermore, combining these first two steps (falling in air and entering water) has a calculated duration similar to experimentally found times between the molten-metal/water contact and fragmentation. The idea of Witte et al. [42]—initial vapor film collapse causes fragmentation—still remains valid. Moreover, the assumption of direct contact between the melt and the coolant results in similar heat fluxes as experimentally found by Board et al. [89], suggesting the validity of this assumption. The model was also used to determine the thickness  $\delta$  of the vapor film. This  $\delta$  corresponds well with experiments, suggesting the validity of the model. The model for  $\delta$  is represented in Figure 18 as a function of a dimensionless time  $\bar{\tau}$  for varying angular locations  $\theta$ . The main observations include:

- Angular locations below  $90^\circ$  do not show a significant difference in vapor film thickness with time (as compared to higher angles).
- The initial vapor film thickness is rather constant, but increases faster and more for higher angles.
- After a certain time, the film thickness reaches a maximum and then starts to decrease.

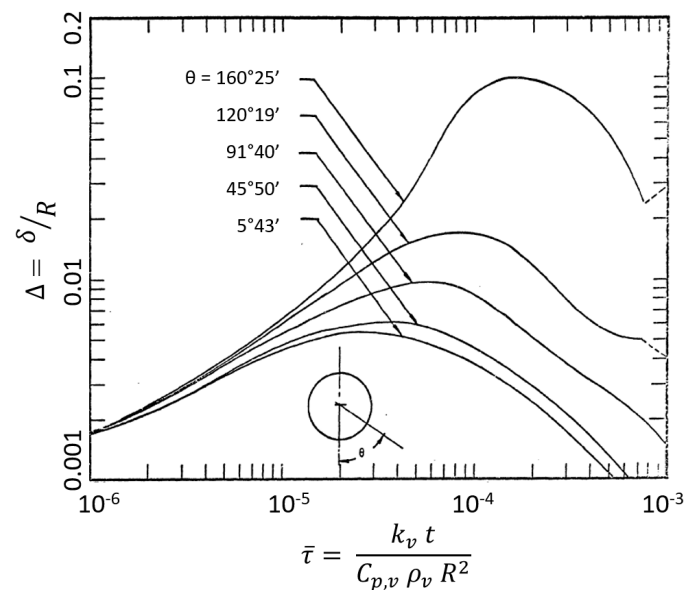


**Figure 18.** Time dependence (dimensionless time  $\bar{\tau}$  on the X-axis) of vapor film thickness  $\Delta$  (represented dimensionless on the Y-axis) for different angular locations  $\theta$  (adapted from Reference [52]).

Lastly, Hsiao et al. [52] mention that they have two new possible mechanisms for fragmentation. The first possibility is based on the cyclic collapse and regrowth of the vapor film, which was experimentally observed by Board et al. [88] prior to fragmentation. As such, it is opted that this cyclic process might cause a pressure imbalance, resulting in the droplet fragmentation. The second possibility is based on the direct contact between the melt and the coolant. At the moment of this direct contact, the heat flux peaks, and the contact temperature suddenly drops to a lower value. As a consequence, the melt will shrink, causing tensile stresses inside the droplet. If these stresses become sufficiently high, they might result in cavitation of the melt and cause fragmentation. This mechanism is an extreme variant of ‘thermal shock’ which was described in Section 2.1.

Since the research of Hsiao et al. [52], multiple transient models were developed [91–94]. One particular model is that of Medhekar et al. [95]. In contrast to the paper of Hsiao et al. [52], which mainly focused on the equations for the temperature field, the velocity field, and the general appearance (i.e., the thickness of the vapor film) during vapor film destabilization, Medhekar et al. [95] focused more on the consequences of the vapor explosion (i.e., the pressure peak and the velocity profile that result from the explosion). The developed model takes into account three phases of which two are liquids (melt/liquid coolant/gaseous coolant). The equations are described in 3D, but the results apply to a 1D simulation for different melt compositions into water. The reader is referred to the paper of Medhekar et al. [95] for a complete overview of their model. Some of the results can be seen in Figure 19. There, the pressure profiles following the interactions between different melts and water are represented. The initial conditions for these simulations can be found in Table 3. The water was always at its boiling temperature and  $T_{hot}$  was similar for all experiments, except for the one with thermite, since iron has a higher melting temperature (1538 °C [62]). It should be noted that the radius of the melt droplet was always the same, but the total volume was varied as to change the volume fraction of the melt. This change in total volume causes a change in energy density between the two cases with tin. The total amount of vapor was varied to investigate the influence of the vapor void fraction in cases tin(A) versus tin(B), which could be a representation of the influence of the moment of triggering. Finally, the amplitude of the trigger was varied for the different melts depending on the stability of the system. It can be seen that tin(B) used a larger trigger than tin(A); this is because the larger vapor void fraction causes the vapor film to be more stable in case of tin(B).

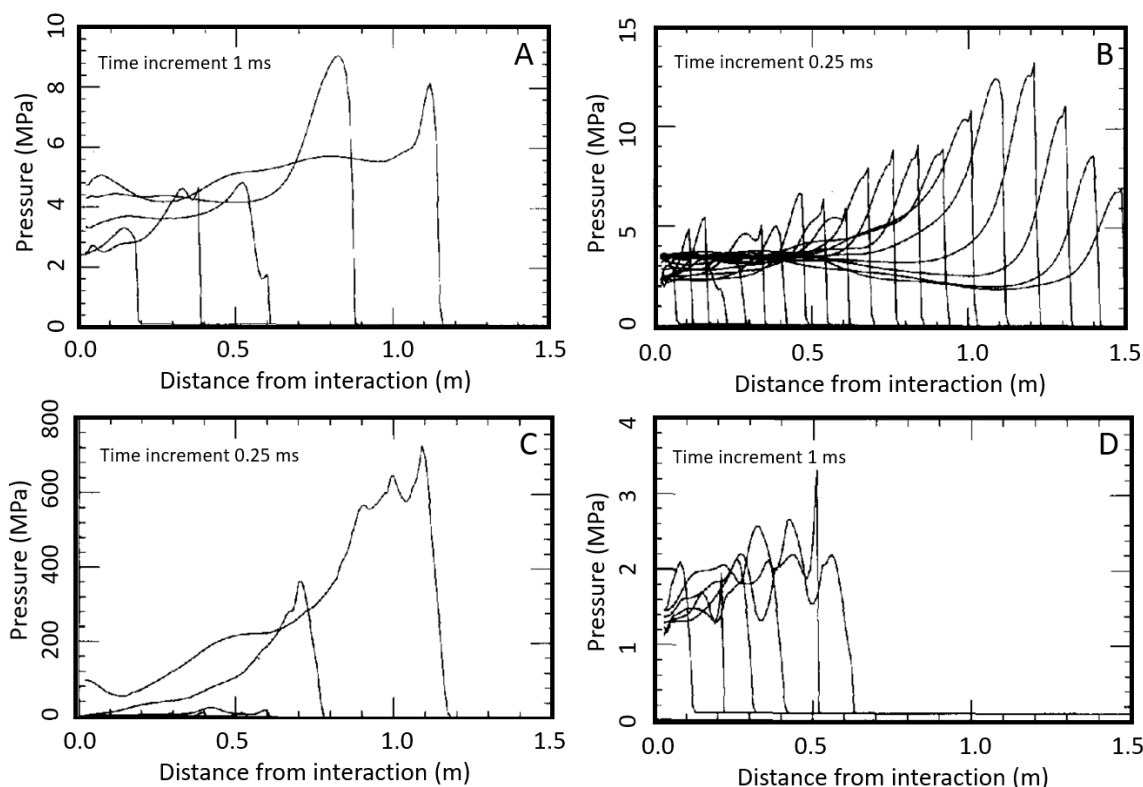


**Figure 19.** Calculated pressure profiles for different melts in water: (A) tin(A); (B) aluminum; (C) thermite; (D) tin(B) (adapted from Reference [95]).

**Table 3.** Relevant initial conditions for the calculations of Reference [95] (cfr. Figure 19).

| System   | Tin(A)-H <sub>2</sub> O | Thermite-H <sub>2</sub> O | Al-H <sub>2</sub> O | Tin(B)-H <sub>2</sub> O |
|--|-------------------------|---------------------------|---------------------|-------------------------|
| Pressure (MPa)                                 | 0.1                     | 0.1                       | 0.1                 | 0.1                     |
| Hot phase temperature (K)                      | 1123                    | 2500                      | 1273                | 1123                    |
| Water temperature (K)                          | 373                     | 373                       | 373                 | 373                     |
| Hot phase volume fraction                      | 0.4                     | 0.3                       | 0.3                 | 0.2                     |
| Vapor void fraction                            | 0.1                     | 0.1                       | 0.1                 | 0.2                     |
| Hot phase drop radius (m)                      | 0.005                   | 0.005                     | 0.005               | 0.005                   |
| Trigger ( $\times 10^6$ kg/(m <sup>3</sup> s)) | 40                      | 16                        | 12                  | 50                      |
| Energy content (cal/cm <sup>3</sup> )          | 153                     | 574                       | 157                 | 77                      |

The peak pressures in Figure 19 show that the maximum value increases with the energy density of the experiment, as does the distance after which this maximum is obtained. This is because a higher pressure corresponds with a faster traveling wave, which can be observed by counting the time increments in the different images (which also applies to explosions in air [96]). Lastly, Medhekar et al. [95] mention that even with a larger trigger, the case of tin(B) could not escalate into an explosion, even though both cases with tin result in similar coolant velocities and fragmentation rates.

Lastly, it should be mentioned that Medhekar et al. [95] mention themselves that their simulations are not perfect since the initial conditions are not realistic (e.g., concentric cylindrical vapor layer in simulation, whereas reality has a concentric conical shaped vapor layer (i.e., a vertical combination of tin(A) and tin(B))). More work is needed to improve these kinds of models, but they do argue that this approach is able to investigate the steps that occur in vapor explosions after triggering.

This study, together with many others, was the basis for current research in the modeling of vapor explosions. As a specific example, Berthoud [8] mentions that the model of Medhekar et al. [95] is one of the models that is similar to IDEMO, a parametric model

developed by Carachalios et al. [97]. In a more recent paper, Meignen [9] reviewed some of the existing parametric models, including IDEMO. This shows that the current models had their roots in the models that were developed long ago. These more recent parametric models are out of the scope of this study but prove the relevance of the older models.

## 5. Conclusions and Outlook

The scope of this paper was to investigate vapor explosions in small-scale from a heat transfer point of view, but these fundamental studies are relatively rare in more recent studies, as compared to a few decennia in the past. We believe that the impact of these older and more fundamental studies are currently being underestimated. With this review paper, we hope to revitalize these more fundamental investigations, but we want to emphasize that all recent studies discussed in our review paper are also important in the development of our understanding of vapor explosions. These more recent papers sometimes tackled specific problems from a more applied point of view and are, thus, very relevant for industry. For instance, specific compositions have been investigated both in the present and in the past, but it seems like there is no knowledge about the exact influence of a variable composition outside of the previously investigated ranges. Even though, today, industries have more direct benefits from the more practical research that is currently being performed, we have the opinion that a better understanding of the fundamental behavior of vapor explosions will result in new insights in how to prevent vapor explosions with severe consequences. This paper gave a review of the relevant fundamental studies carried out from a heat transfer point of view, which can be used as a basis for further fundamental research.

The interaction between a liquid hot phase and a liquid coolant could lead to a vapor explosion. It was mentioned that such a vapor explosion for experiments with droplet impingement can only occur for certain combination of temperatures of the hot and cold phase (within the temperature interaction zone TIZ). However, the borders of the TIZ seem rather uncertain, as there has been a misunderstanding about the role of the critical temperature of the coolant at these borders. Further research would certainly be valuable on this specific topic. Furthermore, in these experiments with a liquid coolant and a liquid hot phase, it is hard to focus on the transition temperature as it is no longer possible to put a thermocouple inside the hot phase during the experiments. From here on, the focus was mainly on whether or not a certain combination of materials and temperatures would cause a vapor explosion, rather than on the characteristics of the heat transfer. The as-such performed experiments with jets could be divided into four categories, depending on their initial conditions for coolant and melt temperature:

- Mode A (cold metal, warm water):  
Film boiling with low vapor production rate, stable penetration and break-up, no explosion.
- Mode B (medium metal, warm water):  
Periods of film boiling interrupted by coherent breakdown of the film, real vapor explosion.
- Mode C (warm metal, warm water):  
Film boiling above the critical temperature of water, delayed break-up, no explosion.
- Mode D (medium metal, cold water):  
Nucleate or transition boiling (no stable film), no penetration, rapid small explosions.  
Mode B was argued to be the most severe kind of vapor explosion since the high water temperature allowed for some penetration of the melt in the coolant. As such, all energy could be released at once rather than being immediately released at the first contact with the water (Mode D), which is more similar to what happens in experiments with droplet impingement.

Research towards heat transfer started approximately 70 years ago. Most initial studies were about the heat transfer coefficient  $h$  (or the Nusselt number  $Nu$ ) between a hot solid surface and water at its boiling point. As such, by neglecting radiation, it could be assumed that all heat was transferred from the surface towards the vapor layer. Any heat passing through the vapor layer will result in evaporation of the surrounding liquid, resulting in the addition of heat to the vapor layer rather than to the surrounding liquid. Variations were investigated in the shape of the surface and the kind of convection. Later studies varied the coolant temperature to not solely focus on coolants at their boiling temperature. The following relations were found [73,74,77–81,83]:

- $Nu$  (related to heat transfer coefficient) increases with decreasing coolant temperature.
- $Nu$  increases with decreasing temperature of the hot phase.
- $Nu$  increases with increasing Reynolds number  $Re$ . At low  $Re$ , the influence of the temperature of all phases is rather important, but it loses importance as  $Re$  is increased.
- The heat flux leaving the hot phase increases with increasing relative velocity.
- The heat flux increases with an increase in the initial temperature of the hot phase.
- The transition temperature increases as a function of the initial temperature of the hot phase.
- The relative velocity does not have an influence on the transition temperature.
- The transition temperature decreases with increasing coolant bulk temperature.
- The highest heat flux in nucleation boiling increases with decreasing coolant temperature.
- The temperature range for transition boiling moves to higher temperatures for colder surrounding liquid. The temperature of the hot phase resulting in the minimum heat flux increases linearly with decreasing coolant temperature.
- The heat flux at transplosion is independent of the initial sphere temperature. When the bulk temperature of the coolant decreases, the critical heat flux increases.

The temperature at the moment of transition from film boiling to transition boiling is referred to as the transition temperature. In the case of a thermal instability of the film, this temperature corresponds to the minimum film boiling temperature  $T_{MFB}$  and was investigated both experimentally and theoretically. Earlier theoretical studies [55,56] revealed two different manners to determine  $T_{MFB}$ : a thermal model and a hydrodynamic model.  $T_{MFB}$  in the thermal model (small amount of hot phase with low relative velocity) is independent (or weakly dependent) on the material used as the hot phase. Furthermore, it was found that the thermal model only shows minor changes when the input properties are varied (hence, minor influence of the used material), whereas the hydrodynamic model shows a major change. It was concluded that the hydrodynamic model has the upper hand (over the thermal model), whenever it is applicable. In case it is not applicable, thermal effects might still destabilize the vapor film. Further research is required to determine when the hydrodynamical model is applicable, thus investigating the influence of the destabilizing properties (e.g., the relative velocity) on the triggerability of vapor explosions outside of the TIZ.

A diagram of coolant temperature versus hot phase temperature was used when investigating the phenomena occurring during cooling. Initially, the hot phase was a small sphere which was moving through a large tank of water. The following observations were made [66]:

- The vapor film was thick/stable when the sphere and the coolant were at a high temperature.
- The film remained thick when the initial temperature of the hot phase was decreased until the vapor film became unstable. On the other hand, the film became thinner and showed irregularities when the initial coolant temperature was decreased. In that case, cooling of the hot phase resulted in a progressive transition from film boiling to transition boiling.
- When both initial temperatures were decreased, a thin and smooth vapor film was observed. Cooling of the hot phase was followed by an abrupt change of film boiling to

transition boiling (a transposition). The line representing the transposition was defined as that line where the heat flux equals a minimum heat flux to sustain film boiling. The higher the coolant temperature, the lower the minimum heat flux to sustain film boiling.

Initially, researchers observed that the initial temperature of the hot phase is directly proportional with the transition temperature [81]. However, later experiments often used a single hot phase temperature [16,83]. Moreover, theoretical studies often assumed steady-state. As such, no transient system could be investigated and the influence of the initial temperature was ignored. Further investigating of this dynamic behavior of the vapor film could result in a better understanding about the moment and way of triggering of vapor explosions, resulting in a possible better prevention of severe accidents. The easiest way to investigate the transient behavior is to further explore the influence of the initial temperature on the timing of the vapor explosion. In addition, modeling of heat transfer could be used to estimate the temperature of the melt at the moment of the interaction.

Lastly, some transient models were discussed. It was explained that these models are important in getting a better understanding about the dynamics of both heat transfer and the vapor film, thus in determining which of these processes has the shortest time constant. This was important to determine whether the vapor film can be assumed in a quasi-steady-state during experiments. The first model was used to investigate the behavior of the vapor film during film boiling. It was explicitly mentioned that the vapor film might collapse locally, and the growth and collapse of the film can clearly be observed for different positions around the droplet. A more recent model was discussed afterwards, simulating the behavior after a steam explosion. Focus was laid on the pressure and velocity profile following a vapor explosion, revealing that a larger vapor void fraction at the moment of triggering results in more stable film boiling and inhibits vapor explosions. Furthermore, it seems that the maximum value of the peak pressure increases with increasing initial energy content. Further research would be valuable to confirm/improve these transient models.

**Author Contributions:** Conceptualization, A.S., I.B., and T.C.; investigation, A.S.; methodology, A.S.; project administration, I.B., T.C., and K.V.; supervision, I.B., T.C., and K.V.; validation, A.S.; resources, A.S.; writing—original draft, A.S.; review & editing, I.B., T.C., and K.V. All authors have read and agreed to the published version of the manuscript.

**Funding:** This work was supported by VLAIO, the Flanders Innovation & Entrepreneurship Agency, in co-operation with Umicore under Grant HBC.2018.0208. I. Bellemans holds a research grant from the Research Foundation—Flanders (12Z7720N).

**Institutional Review Board Statement:** Not applicable.

**Informed Consent Statement:** Not applicable.

**Data Availability Statement:** Not applicable.

**Conflicts of Interest:** The authors declare no conflict of interest.

## Abbreviations

| Symbol            | Definition   |
|-------------------|--|
| $A_t$             | Atomic weight [kg/mol]   |
| $C_{p,i}$         | Heat capacity of phase i [J/(kg·K)]                                  |
| $D$               | Outside diameter of tube/sphere/droplet [m]                          |
| $g$               | Local acceleration of gravity [m/s <sup>2</sup> ]                    |
| $h$               | Heat transfer coefficient [W/(K·m <sup>2</sup> )]                    |
| $\Delta H_{evap}$ | Enthalpy of evaporation [J/kg]                                       |
| $k_i$             | Thermal conductivity coefficient of phase i [W/(K·m)]                |
| $P$               | Pressure [Pa]  |
| $q$               | Heat flux per unit of area [W/m <sup>2</sup> ]                       |
| $R$               | Radius of the tube/sphere/droplet [m]                                |
| $T_i$             | The temperature of phase i [K]                                       |
| $U_\infty$        | The relative velocity between the hot phase and the cold phase [m/s] |

|               |   |
|---------------|---|
| $\delta$      | Thickness of vapor layer [m]  |
| $\epsilon_i$  | Emissivity factor of phase i [-]  |
| $\theta'$     | The angle at which vapor layer detaches from the hot phase [-]  |
| $\lambda'$    | The difference in enthalpy between vapor at its average temperature and liquid at its boiling point (approximately equal to latent heat) [J/kg] |
| $\mu_i$       | Dynamic viscosity of phase i [Pa·s]   |
| $\rho_i$      | The density of phase i [kg/m <sup>3</sup> ]   |
| $\sigma$      | Surface tension [J/m <sup>2</sup> ]   |
| $\sigma_{sb}$ | Stefan-Boltzmann constant [5.667 W/(m <sup>2</sup> ·K <sup>4</sup> )]   |
| $Nu$          | Nusselt number: ratio of convective to conductive heat transfer [-]   |
| $Re$          | Reynolds number: ratio of inertial forces to viscous forces [-]   |
| $Pr$          | Prandtl number: ratio of momentum diffusivity to thermal diffusivity [-]  |
| $Sh$          | Dimensionless superheating [-]  |
| $Sc$          | Dimensionless subcooling [-]  |
| Subscripts    |   |
| <i>boil</i>   | boiling   |
| <i>conv</i>   | convection  |
| <i>crit</i>   | critical point  |
| <i>evap</i>   | evaporation   |
| <i>hot</i>    | Hot phase (e.g., melt droplet)  |
| <i>HN</i>     | Homogeneous nucleation  |
| <i>i</i>      | interface   |
| <i>ini</i>    | initial   |
| <i>l</i>      | Liquid coolant  |
| <i>Leid</i>   | Leidenfrost (thermal transition temperature for discrete droplet)   |
| <i>MFB</i>    | Minimum Film Boiling (thermal transition temperature for submerged plate)   |
| <i>r</i>      | radiation   |
| <i>sub</i>    | Subcooling (i.e., difference between $T_l$ and coolant boiling point)   |
| <i>tot</i>    | total   |
| <i>trans</i>  | transition  |
| <i>v</i>      | vapor/gaseous coolant   |

## References

- Dinçer, I.; Zamfirescu, C. *Drying Phenomena: Theory and Applications*; John Wiley and Sons Ltd.: West Sussex, UK, 2016.
- Fauske, H.K. On the mechanism of uranium dioxide-sodium explosive interactions. *Nucl. Sci. Eng.* **1973**, *51*, 95–101. [[CrossRef](#)]
- Leskovar, M.; Meignen, R.; Brayer, C.; Bürger, M.; Buck, M. Material Influence on Steam Explosion Efficiency: State of Understanding and Modelling Capabilities. In Proceedings of the 2nd European Review Meeting on Severe Accident Research, Karlsruhe, Germany, 12–14 June 2007; p. 16.
- Ferguson, S.; Zsomboky, N. Electric arc furnace explosions: A deadly but preventable problem. In Proceedings of the 2017 AISTech Conference, Nashville, TN, USA, 8–11 May 2017; pp. 30–35.
- Epstein, S.G. Molten metal explosions are still occurring. In Proceedings of the Technical Sessions Presented by the TMS aluminium Committee at the TMS 2009 Annual Meeting and Exhibition, San Francisco, CA, USA, 15–19 February 2009; pp. 665–666.
- Reid, R.C. Rapid phase transitions from liquid to vapor. *Adv. Chem. Eng.* **1983**, *12*, 105–208.
- Hildal, K. *Steam Explosions During Granulation of Si-rich Alloys: Effect of Al- and Ca-additions*; NTNU Norwegian University of Science and Technology: Trondheim, Norway, 2002.
- Berthoud, G. Vapor explosions. *Annu. Rev. Fluid Mech.* **2000**, *32*, 573–611. [[CrossRef](#)]
- Meignen, R.; Magallon, D.; Bang, K.H.; Berthoud, G.; Basu, S.; Burger, M.; Buck, M.; Corradini, M.L.; Jacobs, H.; Naitoh, M.; et al. Comparative review of FCI computer models used in the OECD-SERENA program. In Proceedings of the ICAPP, International Congress on Advances in Nuclear Power Plants, Seoul, Korea, 15–19 May 2005; p. 13.
- Meignen, R.; Raverdy, B.; Buck, M.; Pohlner, G.; Kudinov, P.; Ma, W.; Brayer, C.; Piluso, P.; Hong, S.-W.; Leskovar, M.; et al. Status of steam explosion understanding and modelling. *Ann. Nucl. Energy* **2014**, *74*, 125–133. [[CrossRef](#)]
- Shen, P.; Zhou, W.; Cassiaut-Louis, N.; Journeau, C.; Piluso, P.; Liao, Y. Corium behavior and steam explosion risks: A review of experiments. *Ann. Nucl. Energy* **2018**, *121*, 162–176. [[CrossRef](#)]
- Fauske, H.K.; Henry, R.E. *Experimental Technical Bases for Evaluating Vapor/Steam Explosions in Nuclear Reactor Safety*, 1st ed.; American Nuclear Society: Chicago, IL, USA, 2017.
- Fletcher, D. Steam explosion triggering: A review of theoretical and experimental investigations. *Nucl. Eng. Des.* **1995**, *155*, 27–36. [[CrossRef](#)]

14. Furuya, M.; Arai, T. Prescription for use of vapor explosion retardant into salt water. In Proceedings of the 16th International Heat Transfer Conference, Beijing, China, 10–15 August 2018; pp. 2439–2446. [CrossRef]
15. Zielinski, S.M.; Sansone, A.A.; Ziolkowski, M.; Taleyarkhan, R.P. Prevention and Intensification of Melt-Water Explosive Interactions. *J. Heat Transf.* **2011**, *133*, 071201. [CrossRef]
16. Hansson, R.C.; Park, H.S.; Dinh, T.N. Dynamics and preconditioning in a single-droplet vapor explosion. *Nucl. Technol.* **2008**, *167*, 223–234. [CrossRef]
17. Furuya, M.; Arai, T. Effect of surface property of molten metal pools on triggering of vapor explosions in water droplet impingement. *Int. J. Heat Mass Transf.* **2008**, *51*, 4439–4446. [CrossRef]
18. Sibamoto, Y.; Kukita, Y.; Nakamura, H. Small-scale experiment on subcooled water jet injection into molten alloy by using fluid temperature-phase coupled measurement and visualization. *J. Nucl. Sci. Technol.* **2007**, *44*, 1059–1069. [CrossRef]
19. Greene, G.A.; Klein, J.; Klages, J.; Schwarz, E.; Sanborn, Y. Some observations on simulated molten debris-coolant layer dynamics. In Proceedings of the International Meeting on Light-Water Reactor: Severe Accident Evaluation, Cambridge, MA, USA, 28 August–1 September 1983; p. 13.
20. Kourayem, N.; Li, E.; Thoroddsen, S.T. Formation of microbeads during vapor explosions of Field’s metal in water. *Phys. Rev. E* **2016**, *93*. [CrossRef] [PubMed]
21. Efstathios, M.; Clayton, T.C.; John, D.S. *Multiphase Flow Handbook*, 2nd ed.; CRC Press: Boca Raton, FL, USA, 2016.
22. Furuya, M.; Kinoshita, I. Effects of polymer, surfactant, and salt additives to a coolant on the mitigation and the severity of vapor explosions. *Exp. Therm. Fluid Sci.* **2002**, *26*, 213–219. [CrossRef]
23. Leskovar, M.; Uršič, M. Estimation of ex-vessel steam explosion pressure loads. *Nucl. Eng. Des.* **2009**, *239*, 2444–2458. [CrossRef]
24. Strandberg, M. *Ex-Vessel Steam Explosion Analysis with MC3D*; Electronic Research Report; VTT Technical Research Centre of Finland Ltd.: Helsinki, Finland, 2016; ISBN 978-87-7893-460-4.
25. Li, Y.; Wang, Z.; Lin, M.; Zhong, M.; Zhou, Y.; Yang, Y. Experimental studies on breakup and fragmentation behavior of molten tin and coolant interaction. *Sci. Technol. Nucl. Install.* **2017**, *2017*, 1–14. [CrossRef]
26. Witte, L.C.; Cox, J.E.; Bouvier, J.E. The vapor explosion. *JOM* **1970**, *22*, 39–44. [CrossRef]
27. Sallack, J.A. An Investigation of Explosions in the Soda Smelt Dissolving Operations. Canadian Pulp and Paper Association Meeting, Quebec, Canada. 1955, p. 56. Available online: [https://www.researchgate.net/publication/285480721\\_An\\_Investigation\\_of\\_Explosions\\_in\\_the\\_Soda\\_Smelt\\_Dissolving\\_Operations](https://www.researchgate.net/publication/285480721_An_Investigation_of_Explosions_in_the_Soda_Smelt_Dissolving_Operations) (accessed on 28 December 2020).
28. Elgert, J.O.; Brown, A.W. *In-Pile Molten-Metal Water Reactions*; U.S. Atomic Energy Commission: Washington, DC, USA, 1956.
29. Long, G. Explosion of molten aluminum in water—Cause and prevention. *Met. Prog.* **1957**, *71*, 107–112.
30. Rightley, M.; Beck, D.; Berman, M. *Npr/fci Exo-fits Experiment Series Report*; Sandia National Laboratories: Albuquerque, NM, USA, 1993.
31. Page, F.M.; Chamberlain, A.T.; Grimes, R. The safety of molten aluminium-lithium alloys in the presence of coolants. *J. Phys. Colloq.* **1987**, *48*, C3-63–C3-73. [CrossRef]
32. Hess, P.D.; Brondyke, K.J. Causes of molten aluminum-water explosions and their prevention. *Met. Prog.* **1969**, *95*, 93–100.
33. Lemmon, W. Explosions of molten aluminium and water. In Proceedings of the Technical Sessions Sponsored by the TMS Light Metals Committee at the 109th AIME Annual Meeting, Las Vegas, NV, USA, 24–28 February 1980; pp. 817–836.
34. Nelson, L.S.; Eatough, M.J.; Guay, K.P. Why does molten aluminum explode at underwater or wet surfaces? In Proceedings of the Technical Sessions by the TMS Light Metals Committee at the 118th TMS Annual Meeting, Las Vegas, NV, USA, 27 February–3 March 1989; pp. 1057–1067.
35. Page, F.M. Base triggered FCI in copper/water systems. In Proceedings of the Fourth CSNI Specialist Meeting on Fuel-Coolant Interaction in Nuclear Reactor Safety, Bournemouth, UK, 2–5 April 1979.
36. Epstein, L.F. *Metal-Water Reactions. VI. Analytical Formulations for the Reaction Rate*; Technical Report; U.S. Atomic Energy Commission: Washington, DC, USA, September 1959.
37. Higgins, H.M. The Reaction of Molten Uranium and Zirconium Alloys with Water. Interim Summary Report from March 15, 1955 through March 15, 1956; Aerojet General Report No. Agc-AE-7, April 1965. Available online: <https://www.osti.gov/biblio/4361537> (accessed on 28 December 2020).
38. Swift, D. *Semi-Annual Report ANL-7125*; Argonne National Laboratory, Chemical Engineering Division: Lemont, IL, USA, 1965.
39. Brauer, F.E.; Green, N.W.; Mesler, R.B. Metal/water explosions. *Nucl. Sci. Eng.* **1968**, *31*, 551–554. [CrossRef]
40. Hinze, J.O. Critical speeds and sizes of liquid globules. *Appl. Sci. Res.* **1948**, *A1*, 273–288. [CrossRef]
41. Chemical Engineering Division. *Semi-Annual Report ANL-7425*; Argon National Laboratory: Lemont, IL, USA, 1967.
42. Witte, L.C.; Cox, J.E.; Vyas, T.J.; Gelabert, A.A. *The Vapor Explosion—Heat Transfer and Fragmentation IV. Rapid Quenching of Molten Metal*; Technical Report ORO-3936-6; University of Houston: Houston, TX, USA, 1971.
43. Stevens, J.W.; Bullock, R.L.; Witte, L.C.; Cox, J.E. *The Vapor Explosion—Heat Transfer and Fragmentation II. Transition Boiling from Sphere to Water*; Technical Report ORO-3936-3; University of Houston: Houston, TX, USA, 1970.
44. Taleyarkhan, R.P.; Georgevich, V. *Fundamental Experimentation and Theoretical Modeling for Prevention of Molten Aluminum-Water Steam Explosions in Casting Pits*; Oak Ridge National Laboratory: Albuquerque, NM, USA, 1997.
45. Takashima, T.; Iida, Y. A study on the mechanism of spontaneous vapor explosions with single molten tin drops and water. *JSME Int. J. Ser. B Fluids Therm. Eng.* **1995**, *38*, 114–120. [CrossRef]
46. Hsiao, K.H.; Cox, J.E.; Hedgcoxe, P.G.; Witte, L.C. Pressurization of a solidifying sphere. *J. Appl. Mech.* **1972**, *39*, 71–77. [CrossRef]

47. Zyszkowski, W. On the transplision phenomenon and the Leidenfrost temperature for the molten copper-water thermal interaction. *Int. J. Heat Mass Transf.* **1976**, *19*, 625–633. [[CrossRef](#)]
48. Zyszkowski, W. Study of the thermal explosion phenomenon in molten copper-water system. *Int. J. Heat Mass Transf.* **1976**, *19*, 849–868. [[CrossRef](#)]
49. Taleyarkhan, R.P.; Kim, S.; Knaff, C.L. *Understanding Prevention & Mitigation of Molten Metal-Water Explosions in DC Casting Pits*; Technical Report ORNL/TM-13769; Oak Ridge National Laboratory: Oak Ridge, TN, USA, 2000.
50. Bradley, R.H.; Witte, L.C. Explosive interaction of molten metals injected into water. *Nucl. Sci. Eng.* **1972**, *48*, 387–396. [[CrossRef](#)]
51. Simons, A.; Bellemans, I.; Verbeken, K.; Crivits, T. Macroscopic analysis of the reaction between molten copper and water: Simulations and preliminary experiments. In Proceedings of the 58th Annual Conference of Metallurgists, Vancouver, Canada, 18–21 August 2019; p. 14.
52. Hsiao, K.H.; Cox, J.E.; Witte, L.C. *The Vapor Explosion—Heat Transfer and Fragmentation VII. Molten-Metal/Water Interactions Prior to a Vapor Explosion*; Technical Report ORO-3936-11; University of Houston: Houston, TX, USA, 1974.
53. Dullforce, T.A.; Buchanan, D.J.; Peckover, R.S. Self-triggering of small-scale fuel-coolant interactions: I. Experiments. *J. Phys. D Appl. Phys.* **1976**, *9*, 1295–1303. [[CrossRef](#)]
54. Westwater, J.W. Boiling of liquids. *Adv. Chem. Eng.* **1956**, *1*, 1–76.
55. Berenson, P.J. Film-boiling heat transfer from a horizontal surface. *J. Heat Transf.* **2012**, *83*, 351–356. [[CrossRef](#)]
56. Baumeister, K.J.; Simon, F.F. Leidenfrost temperature—Its correlation for liquid metals, cryogenics, hydrocarbons, and water. *J. Heat Transf.* **1973**, *95*, 166–173. [[CrossRef](#)]
57. Kondo, S.; Konishi, K.; Isozaki, M.; Imahori, S.; Furutani, A.; Brear, D. Experimental study on simulated molten jet-coolant interactions. *Nucl. Eng. Des.* **1995**, *155*, 73–84. [[CrossRef](#)]
58. Sibamoto, Y.; Kukita, Y.; Nakamura, H. Visualization and measurement of subcooled water jet injection into high-temperature melt by using high-frame-rate neutron radiography. *Nucl. Technol.* **2002**, *139*, 205–220. [[CrossRef](#)]
59. Giordanengo, B.; Benazzi, N.; Vinckel, J.; Gasser, J.; Roubi, L. Thermal conductivity of liquid metals and metallic alloys. *J. Noncryst. Solids* **1999**, *250*, 377–383. [[CrossRef](#)]
60. Alchagirov, B.B.; Chochoeva, A.M. Temperature dependence of the density of liquid tin. *High Temp.* **2000**, *38*, 44–48. [[CrossRef](#)]
61. Bale, C.; Bélisle, E.; Chartrand, P.; Decterov, S.; Eriksson, G.; Gheribi, A.; Hack, K.; Jung, I.-H.; Kang, Y.-B.; Melançon, J.; et al. FactSage thermochemical software and databases, 2010–2016. *Calphad* **2016**, *54*, 35–53. [[CrossRef](#)]
62. Callister, W.D., Jr.; Rethwisch, D.G. *Materials Science and Engineering*, 9th ed.; John Wiley and Sons, Ltd.: London, UK, 2014.
63. Guo, Z.; Wen, X.; Zhang, S.; Wang, F.; Pan, R.; Sun, Z. Experimental study on the combustion-induced rapid phase transition of syngas/air mixtures under different conditions. *Int. J. Hydrogen Energy* **2020**, *45*, 19948–19955. [[CrossRef](#)]
64. Di Benedetto, A.; Cammarota, F.; Di Sarli, V.; Salzano, E.; Russo, G. Anomalous behavior during explosions of CH<sub>4</sub> in oxygen-enriched air. *Combust. Flame* **2011**, *158*, 2214–2219. [[CrossRef](#)]
65. Di Benedetto, A.; Cammarota, F.; Di Sarli, V.; Salzano, E.; Russo, G. Reconsidering the flammability diagram for CH<sub>4</sub>/O<sub>2</sub>/N<sub>2</sub> and CH<sub>4</sub>/O<sub>2</sub>/CO<sub>2</sub> mixtures in light of combustion-induced rapid phase transition. *Chem. Eng. Sci.* **2012**, *84*, 142–147. [[CrossRef](#)]
66. Stevens, J.; Witte, L. Destabilization of vapor film boiling around spheres. *Int. J. Heat Mass Transf.* **1973**, *16*, 669–670. [[CrossRef](#)]
67. Bejan, A.; Kraus, A.D. *Heat Transfer Handbook*; Wiley: New York, NY, USA, 2003.
68. Aamir, M.; Qiang, L.; Xun, Z.; Wang, H.; Ullah, R. Study on Ultra-fast cooling behaviors of water spray cooled stainless steel plates. *Exp. Heat Transf.* **2016**, *29*, 299–321. [[CrossRef](#)]
69. Motezakker, R.; Sadaghiani, A.K.; Akkoc, Y.; Parapari, S.S.; Gözüaçiği, D.; Kosar, A. Surface modifications for phase change cooling applications via crenarchaeon *Sulfolobus solfataricus* P2 bio-coatings. *Nature* **2017**, *7*. [[CrossRef](#)]
70. Wells, M.A.; Li, D.; Cockcroft, S.L. Influence of surface morphology, water flow rate, and sample thermal history on the boiling-water heat transfer during direct-chill casting of commercial aluminum alloys. *Met. Mater. Trans. A* **2001**, *32*, 929–939. [[CrossRef](#)]
71. Nukiyama, S. The maximum and minimum values of the heat Q transmitted from metal to boiling water under atmospheric pressure. *Int. J. Heat Mass Transf.* **2003**, *9*, 1419–1433. [[CrossRef](#)]
72. Bromley, L.A. *Heat Transfer in Stable Film Boiling*; University of California, Radiation Laboratory: Berkeley, CA, USA, 1948.
73. Bromley, L.A.; Leroy, N.R.; Robbers, J.A. Heat transfer in forced convection film boiling. *Ind. Eng. Chem.* **1953**, *45*, 2639–2646. [[CrossRef](#)]
74. Kobayasi, K. Film boiling heat transfer around a sphere in forced convection. *J. Nucl. Sci. Technol.* **1965**, *2*, 62–67. [[CrossRef](#)]
75. Ganji, D.D.; Sabzehmeidani, Y.; Sedighiamiri, A. (Eds.) *Nonlinear Systems in Heat Transfer: Chapter 3—Radiation Heat Transfer*; Elsevier: Amsterdam, The Netherlands, 2018.
76. Goodfellow, H.; Tähti, E. (Eds.) *Industrial Ventilation Design Guidebook—Chapter 4: Physical Fundamentals*. Academic Press: New York, NY, USA, 2001.
77. Witte, L.C. Film Boiling from a sphere. *Ind. Eng. Chem. Fundam.* **1968**, *7*, 517–518. [[CrossRef](#)]
78. Sparrow, E.M.; Cess, R.D. The Effect of Subcooled Liquid on Laminar Film Boiling. *J. Heat Transf.* **2012**, *84*, 149–155. [[CrossRef](#)]
79. Nishikawa, K.; Ito, T. Two-phase boundary layer treatment of free-convection film boiling. *Trans. Jpn. Soc. Mech. Eng.* **2011**, *31*, 984–991. [[CrossRef](#)]
80. Bradfield, W.S. On the effect of subcooling on wall superheat in pool boiling. *J. Heat Transf.* **2012**, *89*, 269–270. [[CrossRef](#)]
81. Stevens, J.; Witte, L. Transient film and transition boiling from a sphere. *Int. J. Heat Mass Transf.* **1971**, *14*, 443–450. [[CrossRef](#)]

82. Stevens, J.W.; Witte, L.C.; Cox, J.E. *The Vapor Explosion—Heat Transfer and Fragmentation VI. Transient Film and Transition Boiling from a Sphere*; Technical Report No. ORO-3936-9; Atomic Energy Commission: Washington, DC, USA, 1972.
83. Dhir, V.; Purohit, G. Subcooled film-boiling heat transfer from spheres. *Nucl. Eng. Des.* **1978**, *47*, 49–66. [[CrossRef](#)]
84. Henry, R.E. Correlation for minimum wall superheat in film boiling. *Trans. Am. Nucl. Soc.* **1972**, *15*, 420–421.
85. Jouhara, H.; Axcell, B.P. Film boiling heat transfer and vapour film collapse on spheres, cylinders and plane surfaces. *Nucl. Eng. Des.* **2009**, *239*, 1885–1900. [[CrossRef](#)]
86. Matsumura, K.; Nariai, H. Self-triggering mechanism of vapor explosions for a molten tin and water system. *J. Nucl. Sci. Technol.* **1996**, *33*, 298–306. [[CrossRef](#)]
87. Naude, F.; Ellis, A.T. Nonhemispherical cavities collapsing in contact with a solid boundary. *J. Basic Eng.* **1961**, *83*, 648–655. [[CrossRef](#)]
88. Board, S.; Farmer, C.; Poole, D. Fragmentation in thermal explosions. *Int. J. Heat Mass Transf.* **1974**, *17*, 331–339. [[CrossRef](#)]
89. Board, S.; Clare, A.; Duffey, R.; Hall, R.; Poole, D. An experimental study of energy transfer processes relevant to thermal explosions. *Int. J. Heat Mass Transf.* **1971**, *14*, 1631–1641. [[CrossRef](#)]
90. Katz, L.; Sliepcevich, C.M. LNG/water explosions: Cause and effect. *Hydrocarb. Process.* **1971**, *50*, 240–244.
91. Young, M.F. The TEXAS code for fuel-coolant interaction analysis. *Proc. LMFBR Saf. Top. Meet.* **1989**, *3*, 567–575.
92. Fletcher, D.F.; Thyagaraja, A. A mathematical model of melt/water detonations. *Appl. Math. Model.* **1989**, *13*, 339–347. [[CrossRef](#)]
93. Bürger, M.; Miller, K.; Buck, M.; Cho, S.H.; Schatz, A. Analysis of thermal detonation experiments by means of a transient multiphase detonation code. In Proceedings of the 4th International Topical Meeting on Nuclear Reactor Thermal-Hydraulics, Karlsruhe, Germany, 10–13 October 1989; Volume 1.
94. Oh, M.D.; Corradini, M.L. A propagation/expansion model for large scale vapor explosions. *Nucl. Sci. Eng.* **1987**, *95*, 225–240. [[CrossRef](#)]
95. Medhekar, S.; Abolfadl, M.; Theofanous, T. Triggering and propagation of steam explosions. *Nucl. Eng. Des.* **1991**, *126*, 41–49. [[CrossRef](#)]
96. Kinney, G.F.; Graham, K.J. *Explosive Shocks in Air*; Springer Science and Business Media LLC: Berlin/Heidelberg, Germany, 1985.
97. Carachalios, C.; Bürger, M.; Unger, H. A transient two-phase model to describe thermal detonations based on hydrodynamic fragmentation. *Proc. Int. Mtg. LWR Sev. Accid. Eval.* **1983**, *17*, 1–8.